Author manuscript version of article pubished in *Advanced Materials*, **35**, 2023

Control of Enzyme Reactivity in Response to Osmotic Pressure Modulation Mimicking Dynamic Assembly of Intracellular Organelles

Clémence Schvartzman, Hang Zhao*, Emmanuel Ibarboure, Vusala Ibrahimova, Elisabeth Garanger, Sébastien Lecommandoux*

Clémence Schvartzman, Dr. Hang Zhao, Emmanuel Ibarboure, Dr. Vusala Ibrahimova, Dr. Elisabeth Garanger, Prof. Dr. Sébastien Lecommandoux

University of Bordeaux, CNRS, Bordeaux INP, LCPO, UMR 5629, F-33600, Pessac, France.

* Corresponding authors:

E-mail: hangzhao89@hotmail.com; sebastien.lecommandoux@u-bordeaux.fr

Keywords: artificial cells, synthetic organelles, elastin-like polypeptides, microfluidics, liquid-liquid phase separation

Abstract

In response to variations in osmotic stress, in particular to hypertonicity associated with biological dysregulations, cells have developed complex mechanisms to release their excess water, thus avoiding their bursting and death. When water is expelled, cells shrink and concentrate their internal bio(macro)molecular content, inducing the formation of membraneless organelles following a liquid-

Please cite this article as doi: 10.1002/adma.202301856.

liquid phase separation (LLPS) mechanism. To mimic this intrinsic property of cells, functional thermo-responsive elastin-like polypeptide (ELP) biomacromolecular conjugates are herein encapsulated into self-assembled lipid vesicles using a microfluidic system, together with polyethylene glycol (PEG) to mimic cells' interior crowded microenvironment. By inducing a hypertonic shock onto the vesicles, expelled water induces a local increase of concentration and a concomitant decrease of the cloud point temperature (T_{cp}) of ELP bioconjugates that phase separate and form coacervates mimicking cellular stress-induced membraneless organelle assemblies. Horseradish peroxidase (HRP), as a model enzyme, is bioconjugated to ELPs and is locally confined in coacervates as a response to osmotic stress. This consequently increases local HRP and substrate concentrations and accelerates the kinetics of the enzymatic reaction. These results illustrate a unique way to fine-tune enzymatic reactions dynamically as a response to a physiological change in isothermal conditions.

1. Introduction

The cell is the common basic structural and functional unit of every living organism and has fascinated the scientific world for centuries due to its highly complex and multi-compartmentalized structure.[1] Through compartmentalization, cells segregate bio(macro)molecules and control their exchange through selective transport processes, allowing them to modulate the metabolic reactions in time and space that are essential for their function and survival. Each sub-compartment can perform a specific activity without interfering with each other, providing the cell with the unique ability to produce and degrade simultaneously different essential components.[2] Particularly in eukaryotic cells, two distinct types of sub-compartments, called organelles in cellular biology, can be found: one is a subcellular aqueous environment surrounded by a fluidic unilamellar lipid membrane (*e.g.* endosomes, liposomes),[3] while the other is devoid of a lipid boundary and defined as membraneless organelle.[4] The discovery by Brangwynne and co-workers in 2009 of these membraneless organelles has opened a new field of study in cell biology.[5] The existence of membraneless organelles, known as P granules, was evidenced by the interactions between RNA and protein-containing bodies in embryo through a process of liquid-liquid phase separation (LLPS), showing liquid-like characteristics of fusion, dripping and wetting.[5] The underlying mechanism of membrane-free organelle assembly in living cells was associated to the LLPS of RNA and intrinsically disordered proteins (IDPs) under biological signals, such

Please cite this article as doi: 10.1002/adma.202301856.

as changes in cytoplasmic pH, temperature, and osmotic stress.[6] These organelles are consequently able of selective sequestration of biomolecules and catalytic activity, allowing more dynamic and facilitated exchanges with their environment thanks to their lack of membrane.[7] Among biological signals, hyperosmotic stress is a ubiquitous environmental fluctuation in cells, as the number of dissolved molecules in the extracellular environment changes regularly.[8] When subjected to hyperosmotic stress, cells rapidly adapt to volume reduction and simultaneously concentrate internal biomolecules, which can promote the assembly of membraneless organelles capable of guiding and controlling biological responses at the cellular level, which are closely related to neurodegenerative disorders, viral infections, cancers and age-related disorders.[9]

Over the past decade, scientists have made tremendous progress in building, from a bottom-up approach, complex multicompartmental artificial cells as compartments and primitive cells, in order to unveil the origins of life and the mechanisms behind these highly sophisticated systems.[3a, 4b, 10] To understand the assembly of the aforementioned structures and their importance in the proper functioning of natural cells, some research has been carried out to build artificial structures of organelles-in-cells to observe how they assemble, respond to different stimuli and influence the distribution and reactions of biomolecules.[10b, g, 11] However, most of the reported stimuli for organelle assembly so far have generally been easily controlled inducers, such as temperature and electrostatic interactions, and not always biologically relevant. To date, the design of biomimetic systems of biocatalytic membraneless organelles from the LLPS of stimuli-responsive biological materials in artificial cells *via* hyperosmotic stress has not yet been achieved, although some examples have addressed related aspects.[12]

To tackle this challenge, hyperosmotic modulation was chosen as a biologically relevant stimulus for our cytomimetic cellular assemblies. Following a hypertonic shock, we demonstrated the capacity of partially dewetted lipid vesicles to shrink and induce the assembly of synthetic organelles in their crowded lumen. These synthetic organelles resulted from the assembly of specifically designed elastin-like polypeptide (ELP) conjugates where ELP serves as an IDP model, and are either ELP-polymer conjugates or ELP-enzyme conjugates. Horseradish peroxidase (HRP) was selected as a model enzyme because it readily catalyzes the oxidation of amplex red by hydrogen peroxide (H_2O_2) to

Please cite this article as doi: 10.1002/adma.202301856.

fluorescent resorufin, allowing easy monitoring of the reaction kinetics. Our approach has the advantage to be applied in isothermal conditions, avoiding possible artifacts due to temperature change and circumventing any disruption of biological components. We believe our system represents a unique prototype to understand the capacity of cells to respond to osmotic variations, the importance of membraneless organelles towards the activity of cells and the sequestration of biomolecules, and will help to further understand the mechanisms leading to disruptions in LLPS processes.

2. Results and Discussion

2.1. Formation of partially dewetted lipid vesicles and synthetic organelles

Lipid vesicles have been extensively exploited as simplified bottom-up artificial chassis towards cell mimicking.[13] Despite the similarity in their bilayer composition and compartmentalization with those of living cells, lipid vesicles exhibit extremely uncontrollable stability and deformation under hyperosmotic stress, which impairs the accurate estimation of encapsulated components in shrunken vesicles.[14] To this end, we developed liposomes with an attached oil pocket that acts as a lipid reservoir to adjust the volume of the artificial cell compartment, allowing us to study the dynamic process of intracellular LLPS induced by hypertonicity inside these synthetic liposome-based cells.[12] To form the cytomimetic protocellular models, water-in-oil-in-water (W/O/W) double emulsions were prepared using a glass capillary-based microfluidic device (**Figure 1**a). The membranes of liposomes were made from self-assembled Egg PC lipids. To achieve the partially dewetted configuration of as-formed liposomes, 0.2% Pluronic F-68 surfactant was added to the continuous aqueous phase composed of 10 wt% poly(vinyl alcohol) (PVA). This helped to tune and minimize the total interfacial energies between the oil and the external aqueous medium.[10b] Consequently, the oil phase underwent dewetting, but partially remained attached to the vesicles, creating a lipid reservoir that will prevent the vesicles from wildly deforming after an applied hypertonic shock (Figure 1b). As such, stable and partially dewetted liposomes could be observed 15 min after their collection, as seen in Figure 1c.

Please cite this article as doi: 10.1002/adma.202301856.

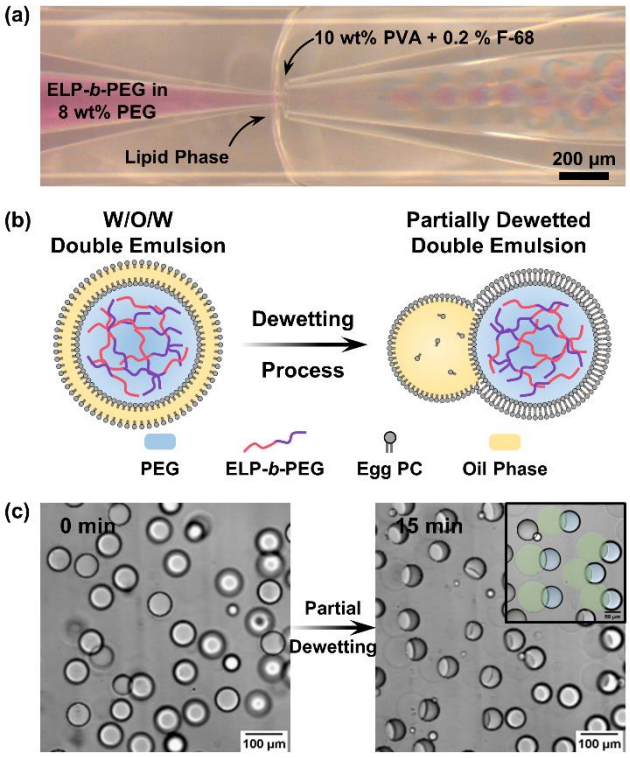

Figure 1. Preparation of W/O/W microdroplet-templated partially dewetted liposomes. (a) Optical image of microfluidic preparation of W/O/W double emulsion microdroplets. (b) Schematic illustration of the transformation of as-formed microdroplets to partially dewetted liposomes. (c) Bright field images observed at t = 0 min showing the freshly collected double emulsion microdroplets, and at t = 15 min revealing the partially dewetted liposomes. Inset: lipid reservoirs are false colored in blue and the lipid vesicles in green. Scale bars denote 100 µm.

To implement the hypertonicity-induced assembly of synthetic organelles within partially dewetted liposomes, a thermosensitive elastin-like polypeptide (ELP) was selected as a core component, which has emerged as a building block to form membraneless organelles mimicking IDPs.[10d, 11a] ELPs are composed of repeating units of a Val-Pro-Gly-Xaa-Gly (VPGXG) pentapeptide sequence and are produced recombinantly in *Escherichia coli* (*E. coli*) bacteria.[15] ELPs exhibit a lower critical solubility temperature (LCST) behavior in water: below their cloud point temperature (T_{cp}), ELP chains are soluble in water, and above the T_{cp} they phase separate and form ELP-rich coacervates.[15-16] Interestingly, the T_{cp} can be tuned mainly by varying the nature of amino acid residues of the

Please cite this article as doi: 10.1002/adma.202301856.

pentapeptide sequence, in particular at the Xaa position, the number of repeat sequences, and the ELP concentration. Here, we specifically focused on a methionine-containing ELP with a primary structure of 40 repeat units of a pentapeptide presenting Val/Met as guest residues in a 3:1 ratio, namely ELP[M_1V_3-40] as reported elsewhere.[17] We chemically conjugated the ELP[M_1V_3-40] to a 2 kDa polyethylene glycol (PEG) yielding the ELP[M_1V_3-40]-*b*-PEG bioconjugate (ELP-*b*-PEG) to form colloidally stable organelle-like compartments.[10c] The ELP-*b*-PEG bioconjugate was fluorescently labeled with rhodamine to enable observation of the spatial distribution of the bioconjugate by fluorescence imaging . To study the dynamic organelle assemblies, the ELP-*b*-PEG bioconjugate (0.25 mg·mL^{-1}) was encapsulated in partially dewetted liposomes together with an 8 wt% PEG solution, mimicking the macromolecular crowded environment of a cell (Figure 1a).[18] A hyperosmotic stress was preferred to a heating system to induce assembly of the synthetic organelles in the newly formed partially dewetted liposomes (**Figure 2**a). This indeed ensured the possibility of assembling synthetic organelles at room temperature inside the cell-mimicking entities, and avoided the inactivation of the future-to-use enzyme. In a first step, we examined the capacity of LLPS of the ELP-*b*-PEG bioconjugate within partially dewetted liposomes by a strong hyperosmotic stress with the addition of a 1 $_M$ sucrose hypertonic solution. Prior to the hypertonic shock, a uniform distribution of ELP-*b*-PEG was observed within the freshly collected lipid compartments (Figure 2b-d). After the hypertonic stress induced by the addition of 1 $_M$ sucrose, partially dewetted liposomes exhibited a rapid reduction in volume to balance the difference in osmotic pressure between the inner and outer environment, instantaneously resulting in the LLPS of the ELP-*b*-PEG bioconjugate into ELP-rich coacervate core micelles as evidenced by the fluorescent aggregates (Figure 2e,f; Figure S1, Supporting Information). As seen in Figure 2g, synthetic membraneless organelle-like constructs spatially distributed in an even manner in the artificial cellular compartment. Significantly, being hit by the hyperosmotic stress, partially dewetted lipid vesicles collectively shrank in volume while maintaining their initial shape, rather than deforming into star-like vesicles or elongated lipid tubes.[14] This confirmed that additional lipids from the shrunken lipid vesicles were fully collected into the lipid reservoirs, offering a new route to precisely govern lipid vesicle size under hypertonic shock. It is noteworthy that the shrunken partially dewetted lipid vesicles are able to reversibly de-shrink in the condition of hypoosmotic stress, swelling closely back to their initial sizes and simultaneously disassemble the organelle-like constructs (Figure S2, Supporting Information).

Please cite this article as doi: 10.1002/adma.202301856.

The effect of hyperosmotic stress upon LLPS of the ELP-*b*-PEG bioconjugate was also investigated at room temperature (23 °C). Hypertonic solutions with increasing concentrations in sucrose (0.25, 0.5, and 1 $_M$) to shrink the partially dewetted liposomes to different extents were explored respectively. The 0.25 $_M$ solution decreased by 35% the initial volume of the lipid vesicles and therefore locally increased the concentration of the ELP-*b*-PEG bioconjugate by a factor of 1.5 (Figure 2h). This condition scarcely assembled synthetic organelles in the lipid vesicles as fluorescently labeled bioconjugates did not show any major aggregation (Figure 2j). The 0.5 $_M$ sucrose solution shrank by 52% the original volume of the lipid compartments, therefore doubling the local concentration in ELP-*b*-PEG, (Figure 2h) which assembled into organelle-like architectures inside the lipid cellular constructs as indicated by fluorescently brighter aggregates of ELP-*b*-PEG conjugates (Figure 2k). Last, the 1 $_M$ sucrose solution was able to reduce by 62% the initial volume of the liposomes and *in situ* surged the local concentration of ELP-*b*-PEG conjugate by 2.6 (Figure 2h). Expectedly, upon hyperosmotic stress with 1 $_M$ sucrose solution, all ELP-*b*-PEG bioconjugates underwent LLPS, assembling a significant population of synthetic membraneless organelles (Figure 2l). These results confirmed that the higher the concentration of the hypertonic sucrose solution, the stronger the hyperosmotic stress exerted on the partially dewetted liposomes, resulting in a higher water efflux that leads to a decrease in vesicle volume. Consequently, the concentration of ELP-*b*-PEG increases locally, inducing the formation of many synthetic subcellular organelles. Indeed, since ELP's cloud point temperature T_{cp} is inversely proportional to their concentration, it can be assumed that the higher the concentration of the hypertonic solution, the greater the shift of T_{cp} of the ELPs to lower temperatures, explaining the observed coacervate formation in isothermal condition as a response to increased concentration (Figure S3, Supporting Information). Noteworthy, hyperosmotic shrinking concentrates not only ELP-*b*-PEG bioconjugates, but also increases the concentration of the macromolecular crowding agent (PEG) which also impacts the shift of T_{cp} to lower temperatures.[10c, d] Considering the combined effect of concentration and macromolecular crowder upon T_{cp} of the ELP-*b*-PEG conjugate, we thus determined the transition temperatures of the resulting three osmotically concentrated ELP-*b*-PEG in their own solution conditions respectively. As evidenced by light scattering experiments (Figure 2i; see experimental details in Supporting Information), ELP-*b*-PEG bioconjugates exhibited a T_{cp} of 34.3 ℃ for the situation with no hyperosmotic shock, that was shifted back to 30 ℃ for a hypertonic shock induced with a 0.25 $_M$ sucrose solution. Since still clearly above ambient temperature, this validated why no synthetic organelle were observed in Figure 2j. With a further increase in sucrose

Please cite this article as doi: 10.1002/adma.202301856.

concentration to 0.5 $_{M}$, the transition temperature shifted to 22.6 °C, and continued shifting to below 10 °C for a 1 $_{M}$ sucrose solution. These measurements are fully consistent with observations from confocal microscopy imaging (Figure 2k,l), attesting the approach of shrinking partially dewetted liposomes is a powerful way to *in vitro* recreate and study the formation of membraneless organelles *via* LLPS in isothermal condition.

Please cite this article as doi: 10.1002/adma.202301856.

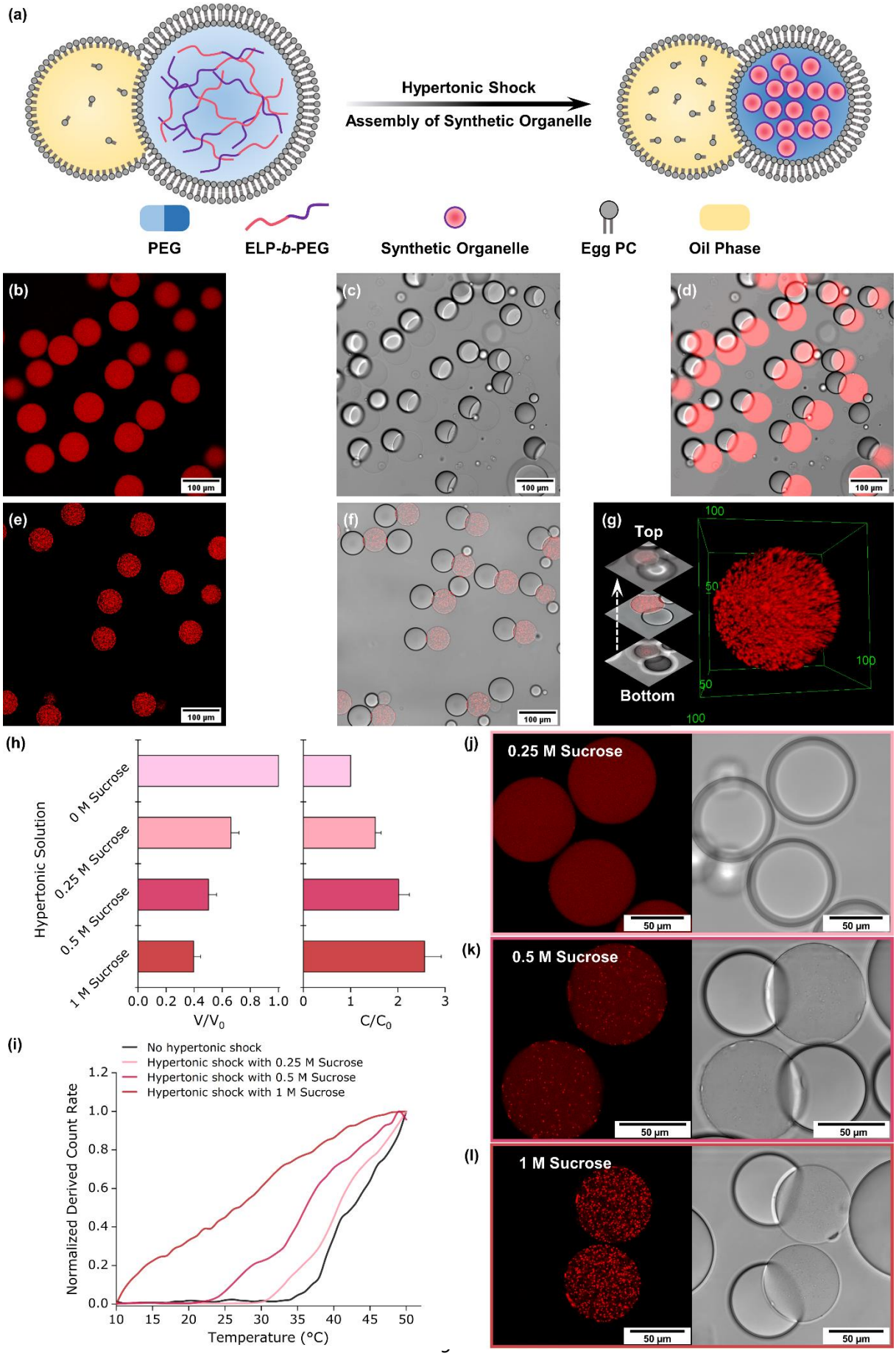
(a)
Hypertonic Shock
Assembly of Synthetic Organelle
PEG
ELP-b-PEG
Synthetic Organelle
Egg PC
Oil Phase
(b)
(c)
(d)
(e)
(f)
(g)
Top
Bottom
100
50
100 µm
(h)
Hypertonic Solution
0 M Sucrose
0.25 M Sucrose
0.5 M Sucrose
1 M Sucrose
0.0 0.2 0.4 0.6 0.8 1.0
V/V0
0 1 2 3
C/C0
(i)
No hypertonic shock
Hypertonic shock with 0.25 M Sucrose
Hypertonic shock with 0.5 M Sucrose
Hypertonic shock with 1 M Sucrose
Normalized Derived Count Rate
0.0 0.2 0.4 0.6 0.8 1.0 1.2
10 15 20 25 30 35 40 45 50
Temperature (°C)
(j)
0.25 M Sucrose
(k)
0.5 M Sucrose
(l)
1 M Sucrose
50 µm

Figure 2. Hypertonicity-triggered assembly of synthetic organelles within partially dewetted liposomes. (a) Schematic illustration of formation of ELP-*b*-PEG synthetic organelles inside cytomimetic lipid compartments in response to hyperosmotic stress. (b-d) Representative confocal images of partially dewetted liposomes with ELP-*b*-PEG encapsulated prior to hypertonic shock, as shown in (b) red channel, (c) bright field and (d) merged channels, respectively. (e-f) Confocal images of as-formed ELP-*b*-PEG synthetic organelles after a 1 $_M$ sucrose hypertonic shock; (e) red channel and (f) merged channels. (g) 3D reconstruction of z-stack confocal images of a partially dewetted lipid vesicle inside of which the ELP-*b*-PEG synthetic organelles are homogeneously distributed. (h) Volume and corresponding concentration ratios of liposomes respectively, depending on the osmolarity of the hypertonic sucrose solutions (n > 30 vesicles). (i) DLS analysis (measurement of the scattered light intensity, also referred to as the normalized derived count rate, DCR) before and after inducing a hypertonic shock allowing the determination of the T_{cp} of ELP-*b*-PEG bioconjugate in different hypertonic conditions. (j-l) Confocal microscopy images represent the efficiency of the various hypertonic sucrose solutions to assemble ELP-*b*-PEG synthetic organelles inside partially dewetted lipid vesicles; (j) 0.25 $_M$, (k) 0.5 $_M$ and (l) 1 $_M$ sucrose.

2.2. Synthetic organelle constructs from co-assembly of ELP-based multicomponent systems

Given that ELP-*b*-PEG bioconjugates are capable of compartmentalizing an ELP-rich hydrophobic coacervate by heating an ELP-based multicomponent system,[10c] we have further here evaluated the potential of hyperosmotic stress to induce similarly the assembly of colloidally stable ELP-based multicomponent systems in partially dewetted lipid vesicles (**Figure 3**a). Similar to our previous report, a BODIPY-labeled monoblock ELP of similar sequence and longer length (BDP-ELP[M_1V_3-60], noted thereafter as BDB-ELP) was chosen to phase-separate and form the ELP-rich coacervate core. An ELP-based multicomponent system of BDP-ELP at 0.5 mg·mL^{-1} and ELP-*b*-PEG at 0.25 mg·mL^{-1} was encapsulated inside partially dewetted lipid compartments. The two fluorophores were found evenly distributed, indicating that both BDP-ELP and ELP-*b*-PEG were in soluble state, as illustrated in Figure 3b1. Shrinking of synthetic cellular compartments *via* a hypertonic solution (1 $_M$ sucrose) gave rise to immediate assembly of ELP-based multicomponent organelle-like structures as evidenced by a clear colocalization of rhodamine and BODIPY dyes grafted onto the ELP-*b*-PEG bioconjugate and

Please cite this article as doi: 10.1002/adma.202301856.

monoblock ELP[M_1V_3-60], respectively (Figure 3b2). These observations of co-assembled complex synthetic organelles from an ELP-based multicomponent system (Figure 3b; Figure S4, Supporting Information) are in good agreement with our previous findings.[10c] To further assess the co-assembly of the system, we also performed dynamic light scattering measurements (DLS) for the three different solutions (BDP-ELP alone; ELP-*b*-PEG alone; and physical mixture of BDP-ELP and ELP-*b*-PEG). As illustrated in Figure 3c, the ELP-*b*-PEG bioconjugate exhibited a cloud point temperature around 33 °C, whereas the T_{cp} of both BDP-ELP and ELP-based multicomponent system were remarkably identical (≈ 23 °C), revealing a high degree of co-assembly of the monoblock ELP and the ELP-*b*-PEG bioconjugate. As such, by means of engaging hyperosmotic stress to shrink our partially dewetted artificial cells, a complex ELP-based multicomponent system can co-assemble into highly organizational and hierarchical subcellular organelle-mimics.

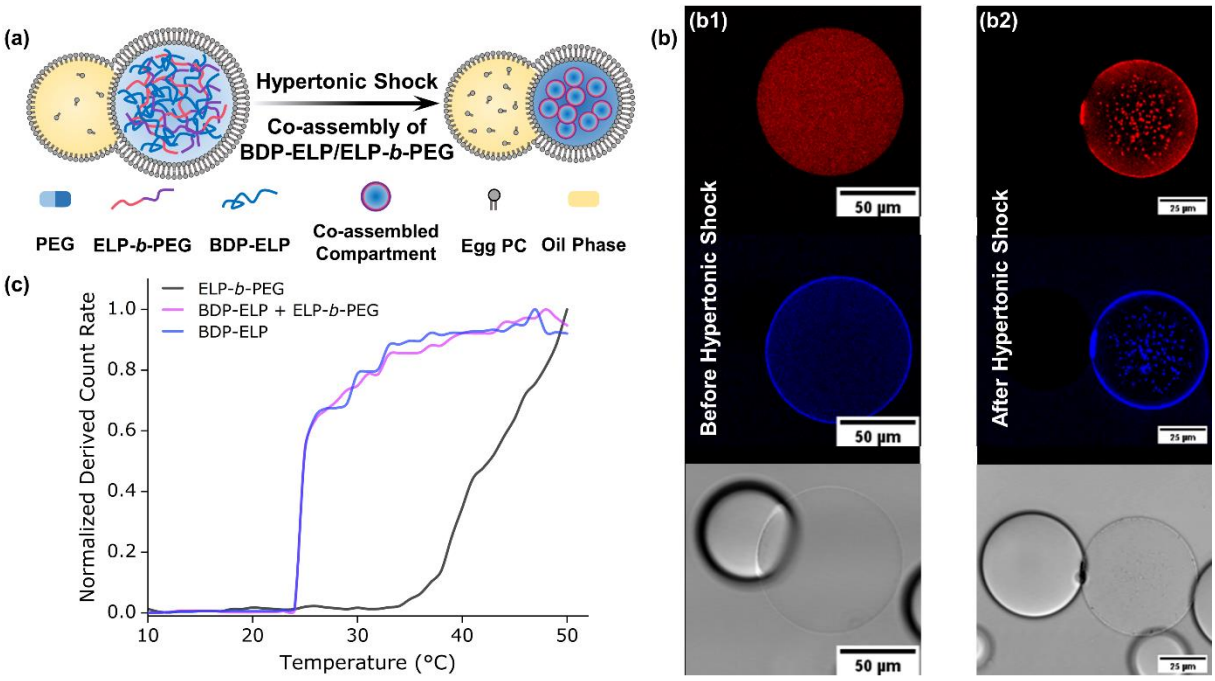

Figure 3. Synthetic organelle constructs from co-assembly of ELP-based multicomponent system. (a) Scheme of co-assembly of the monoblock BDP-ELP and the ELP-*b*-PEG bioconjugate into complex synthetic organelles within shrinking liposomes. (b) Representative confocal microscopy images of ELP-based multicomponent system (BDP-ELP/ELP-*b*-PEG)-containing partially dewetted liposomes before and after hypertonic shock; (b1) no synthetic organelles formed before hypertonic shock and

Please cite this article as doi: 10.1002/adma.202301856.

(b2) co-assembled BDP-ELP/ELP-*b*-PEG into synthetic organelles after hypertonic shock. (c) DLS measurements for the three separate systems verifying the co-assembly mechanism established for the ELP-based multicomponent system.

2.3. Design of synthetic biocatalytic organelles to modulate the kinetics of enzymatic reactions

After assembling complex and colloidally stable synthetic organelles from the ELP-based multicomponent system, we sought to reconstitute a higher level of complexity and functionality (**Figure 4**a). To achieve this, we have designed an ELP-bioconjugate with horseradish peroxidase (HRP) as a model enzyme. A bioengineered ELP[M_1V_3-40] containing a *C*-terminal cysteine group was produced in *E. coli* and coupled to HRP using an heterobifunctional cross-linker 4-(*N*-maleimidomethyl)cyclohexane-1-carboxylic acid 3-sulfo-*N*-hydroxysuccinimide ester (Figure 4b; Figure S5, S6 and S7 and see experimental details in Supporting Information). In order to evaluate the co-assembly ability of biofunctional conjugate ELP-*b*-HRP with the monoblock ELP, we first performed DLS measurements by detecting the cloud point temperatures of the following three solutions in 8 wt% PEG: BDP-ELP alone, ELP-*b*-HRP and BDP-ELP/ELP-*b*-HRP. As seen in Figure 4c, the bioconjugate ELP-*b*-HRP evidenced a transition temperature at 26 °C. However, both transition temperatures of BDP-ELP and BDP-ELP/ELP-*b*-HRP shifted towards the same cloud point temperature around 23 °C, confirming the successful co-assembly of the monoblock ELP and the biofunctional ELP-*b*-HRP conjugate, similar to previous experiments (Figure 3c). We have then used this approach to design a system that combined the three ELP-derived elements, namely the monoblock ELP, the ELP-*b*-PEG and the biofunctional ELP-*b*-HRP conjugate. We could then anticipate conditions where the ELP-*b*-HRP conjugate could be free in solution (before hypertonic shock) or co-assembled in the tripartite coacervate (after hypertonic shock with 1 $_M$ sucrose) at the same ambient temperature (defined as 23 °C). This now allowed us to measure the HRP enzymatic kinetics in these different situations at same temperature and enzyme concentration, both in bulk solution and in partially dewetted liposomes, and evaluate the effect of confinement of the enzyme in organelle-like system, thus mimicking very closely cells' behavior. This kinetics analysis was conducted using the following enzymatic reaction: amplex red was oxidized by H_2O_2 through the catalysis of HRP to produce resorufin as a fluorescent probe (Figure 4a,b). It was ensured that the same concentration of HRP was used between free HRP

Please cite this article as doi: 10.1002/adma.202301856.

and ELP-*b*-HRP for further experiments. The kinetic analysis of ELP-*b*-HRP and HRP was first assessed in bulk solution, in water and in 8 wt% PEG as a crowding agent, which are conditions similar to those in our artificial cells. The co-factor H_2O_2 concentration was first varied. The Michaelis-Menten kinetics for each of these conditions could be determined using equations (Equation S3 and S4, Supporting Information), as well as the Lineweaver Burk plots (Figure S8, see experimental methods in Supporting Information).[19] All calculated values are reported in **Table 1**. In 8 wt% PEG conditions, the K_m of ELP-*b*-HRP decreased 5.7 times compared to water, and 2.9 times for free HRP. This reflected a higher affinity between the substrate and the enzyme, attributed to the increased probability of an interaction between the enzyme and the substrate due to the crowded PEG environment, in agreement with previous reports.[19-20] However, the enzyme's specific activity (*S.A.*) and V_{max} decreased. The *S.A.*, referring to the mole of substrate converted by the enzyme per unit time per mg of the total enzyme,[21] decreased by 9 folds for ELP-*b*-HRP and 5.5 times for free HRP in PEG conditions compared to water. This could be associated with the limited diffusion of the substrate and the enzyme considering the complexity of the PEG solution and its potential interaction with the substrate and/or the enzyme and/or the coacervates.[19, 22] Hence, the crowding capacity of PEG slowed down the kinetics of enzymatic reactions compared to water, but enhanced the affinity between the substrate and the enzyme.

Please cite this article as doi: 10.1002/adma.202301856.

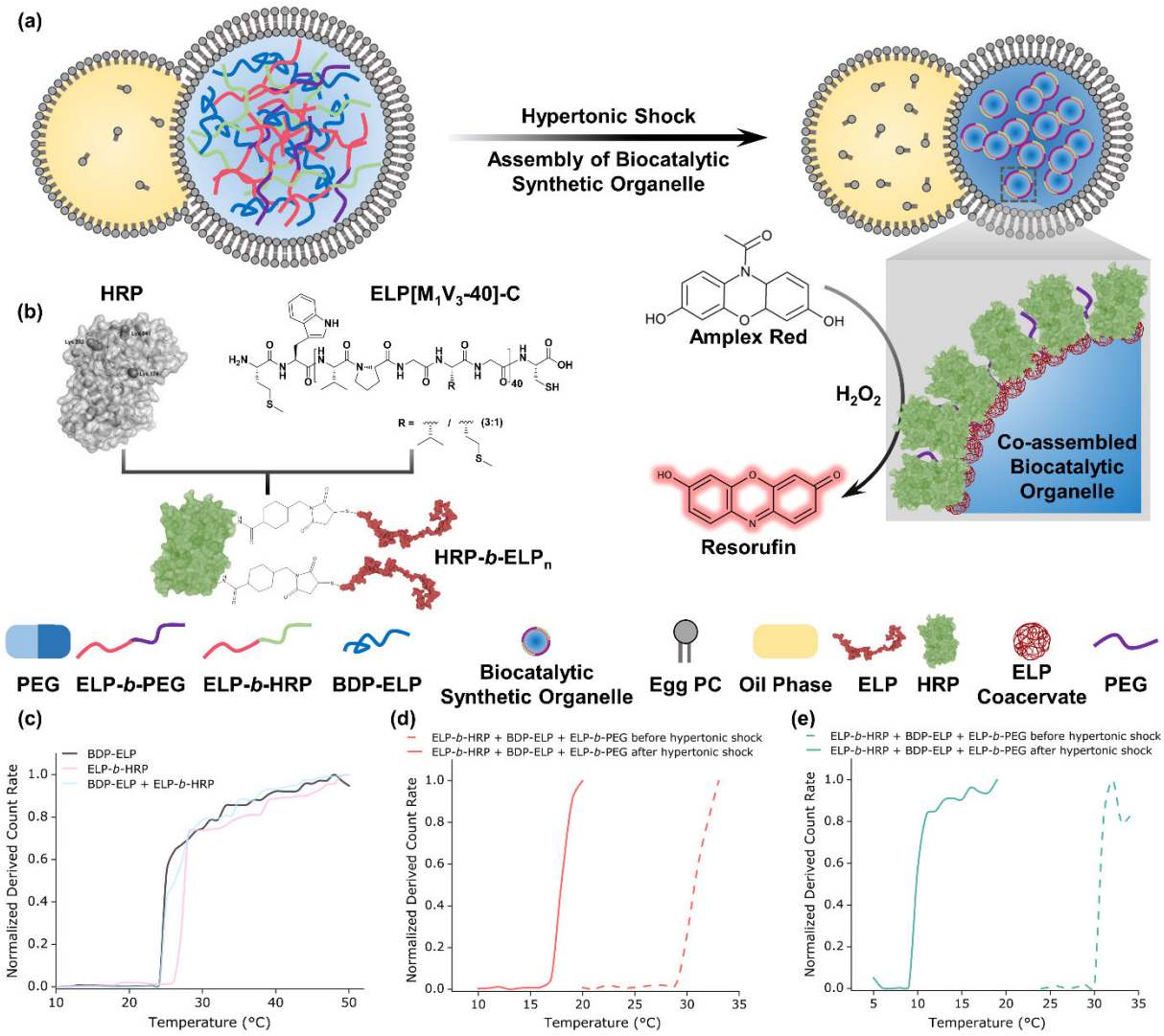

Figure 4. Synthetic catalytic organelles built from co-assembly of a complex ELP-based multicomponent system. (a) Scheme illustrating the shrinking-induced co-assembly of BDP-ELP, ELP-*b*-PEG and ELP-*b*-HRP forming synthetic organelles that are able to catalyze a chemical substrate, amplex red, to a product, resorufin, upon exposure to a chemical fuel of H_2O_2 in the surrounding environment. (b) Schematic representation of the ELP-*b*-HRP bioconjugate design. (c) Determination of co-assembled performance of the ELP-based multicomponent system including BDP-ELP, ELP-*b*-PEG and ELP-*b*-HRP in the solution of 8 wt% PEG. (d) Determination of cloud point temperatures *via* DLS measurements of the ELP-based multicomponent system reproduced the condition in bulk solution before and after in response to hypertonic stress. (e) Determination of cloud point temperatures *via*

Please cite this article as doi: 10.1002/adma.202301856.

DLS measurements of the ELP-based multicomponent system reproduced in the condition occurring inside partially dewetted liposomes before and after in response to hypertonic stress.

Table 1. Michaelis Menten constant (K_m), V_{max}, *S.A.* of ELP-*b*-HRP and HRP in water and 8 wt% PEG, respectively.

Solutions	K_m ($\mu mol \cdot L^{-1}$)	V_{max} ($\mu mol \cdot L^{-1} \cdot s^{-1}$)	*S.A.* ($mmol \cdot g^{-1} \cdot s^{-1}$)
HRP in water	12.5	0.72	0.33
HRP in 8 wt% PEG	4.37	0.13	0.06
ELP-*b*-HRP in water (no coacervates)	22.59	0.71	0.18
ELP-*b*-HRP in 8 wt% PEG (no coacervates)	3.95	0.09	0.02

The kinetics between free HRP and ELP-*b*-HRP were further compared before and after inducing a hyperosmotic stress, to demonstrate the ability of the synthetic organelles to drag and locally increase the concentration of the enzyme and the fluorescent probe. Experiments were first carried out in bulk solution to determine the enzymatic kinetics by fluorescence spectroscopy (see experimental details in Supporting Information). We evaluated the initial and final concentrations of the different compounds as described in the experimental part to mimic the internal environment of vesicles during osmotic variations (Table S1, Supporting Information). DLS analyses were conducted to determine the T_{cp}s of the ELP-based multicomponent system before and after inducing a hypertonic shock. As seen in Figure 4d, the T_{cp}s were detected at 29 ℃ and 16 ℃ respectively, meaning that when performing experiments at 23 °C, the ELP-based multicomponent system will be homogeneously dispersed in initial conditions and will phase separate after a hypertonic shock. Enzymatic reactions were initiated as soon as H_2O_2 was injected into the cuvettes and the increase of fluorescence intensity was monitored (**Figure 5**a). It was observed that, before inducing the hypertonic shock, the kinetics of the

Please cite this article as doi: 10.1002/adma.202301856.

reactions were comparable between the system composed of ELP-*b*-HRP and HRP as the slopes of the curves were similar (**Table 2**). Also, the final fluorescence intensity of the reaction was equivalent in both cases, proving that an equivalent concentration of HRP was used. In the conditions following the hypertonic shock, the slope of the ELP-*b*-HRP curve was much steeper (25.07 ± 3.59 a.u.·s^{-1}) than the one of free HRP (18.26 ± 0.14 a.u.·s^{-1}), suggesting that the formation of synthetic organelles locally concentrated the enzyme and the amplex red, ensuring a faster enzymatic reaction. As a control, an experiment was conducted using the ELP-*b*-PEG conjugate (Figure 5a). No fluorescence could be detected, attesting that no uncontrolled oxidation occurred in our experimental conditions and the presence of HRP was mandatory for a fluorescence signal to be detected. To further support our findings, an alternative chemical substrate 2,2'-azino-bis(3-ethylbenzothiazoline-6-sulphonic acid) (ABTS) was used for the enzymatic reaction with assistance of the enzyme HRP and H_2O_2. The kinetics of ABTS oxidation into its radical cationic blue-colored $ABTS^{\cdot+}$ was determined using UV-Vis spectrophotometer (see experimental details in Supporting Information). Similar enzymatic reaction rates were observed where both ELP-*b*-HRP and free HRP (after hyperosmotic shock) can faster catalyze the oxidation process of ABTS to $ABTS^{\cdot+}$ than conditions with both enzymes freely dispersed in the 8 wt% PEG solution (Figure S9, Supporting Information). Significantly, after hypertonic shock, the ELP-based multicomponent system exhibited a remarkably higher reaction kinetics than that of the free HRP-containing system, reaffirming as-formed biocatalytic synthetic organelles can powerfully enhance the rate of enzymatic reaction.

Table 2. Slope of the fluorescence intensity curves versus time.

Solution	Slope (a.u.·s^{-1}) from (t = 0)
ELP-*b*-HRP after hypertonic shock	25.07 ± 3.59
HRP after hypertonic shock	18.26 ± 0.14
ELP-*b*-HRP before hypertonic shock	12.19 ± 0.79
HRP before hypertonic shock	11.04 ± 0.85

Please cite this article as doi: 10.1002/adma.202301856.

Experiments were then conducted inside partially dewetted vesicles obtained from a microfluidic system and under confocal microscopy. Prior to investigating the performance of enzymatically active synthetic organelles, we examined the permeability of the eventual product (resorufin) to membranes of partially dewetted liposomes (Figure S10, Supporting Information). Partially dewetted liposomes were incubated with resorufin within the same observation chamber. No significant fluorescence intensity increase inside liposomes was observed after monitoring the diffusion of resorufin for 20 min. Thus, this finding validated that the fluorescence intensity changes resulted from the enzymatic reaction within liposomes and not by possible resorufin diffusion due to vesicle bursting in the surrounding environment. A ten times higher concentration of the enzyme was used for both ELP-*b*-HRP-containing multicomponent system and HRP alone system due to intrinsic differences in device sensitivity. This greatly shifted the T_{cp} from 30 ℃ to 9 °C before and after hyperosmotic stress, respectively (Figure 4e). As can be seen in Figure 5b, in conditions of non-shrinking, the increase of fluorescence was very slow and visually imperceptible for both free HRP and the ELP-*b*-HRP system, even 950 s after H_2O_2 injection (Figure S11, Supporting Information). In this case, the HRP that was freely dispersed in the vesicle lumen behaved consistently in both cases, with a slow kinetics as averaged on 14 vesicles (Figure 5b). After a hypertonic shock and a resulting shrinking of partially dewetted vesicles, the production of the fluorescent resorufin could be detected and measured over time (Figure 5b). For free HRP, the resulting increase of enzymatic concentration accelerated the reaction kinetics and a plateau was reached about 1,000 s after H_2O_2 injection (Figure 5b,c; Video S1, Supporting Information). In the case of the ELP-*b*-HRP-containing system, the enzymatic reaction was much faster, with a maximum fluorescence obtained after 250 s only (Figure 5b,c; Video S1, Supporting Information). In the latter case, HRP was confined on the surface of biocatalytic organelle constructs, inducing an increased local concentration of enzyme that enhanced the reaction kinetics. Concomitantly, coacervate formation offered a more hydrophobic environment for amplex red that can also be responsible of a local increased concentration of both enzyme and reactant that can also favor the reaction.[23]

Please cite this article as doi: 10.1002/adma.202301856.

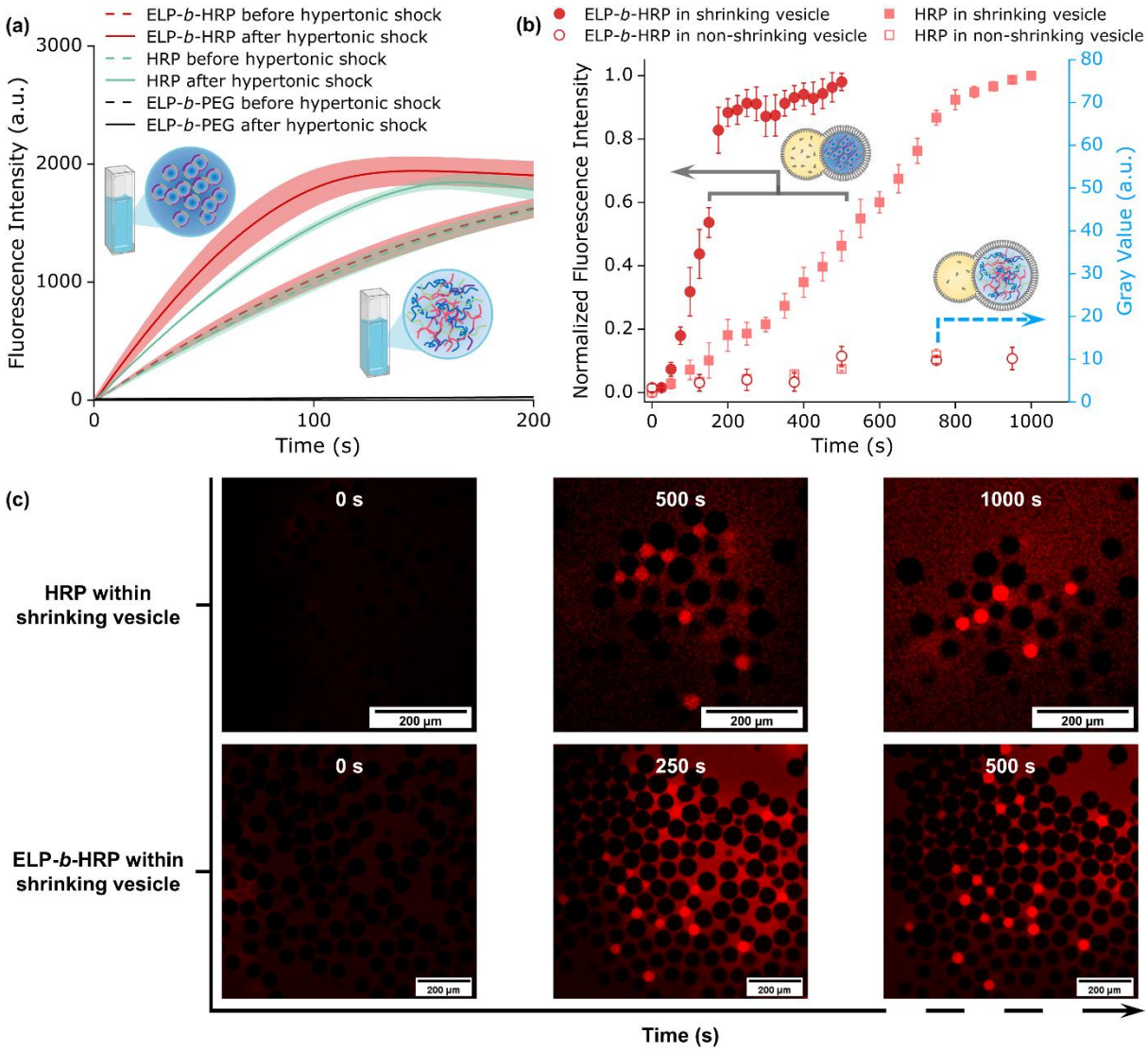

Figure 5. Kinetics of the enzymatic reaction from ELP-based multicomponent system and free HRP system before and after a hypertonic shock, respectively. (a) Kinetics of enzymatic reactions monitored by the increase of fluorescence intensity detected with spectroflurometer. (b) Enzymatic reaction occurring in shrinking and non-shrinking vesicles from ELP-*b*-HRP system and HRP system. (c) Time series of confocal microscopy images in the red channel to follow the formation of resorufin after the hypertonic shock in vesicles encapsulating free HRP and ELP-*b*-HRP system, respectively.

3. Conclusion

Please cite this article as doi: 10.1002/adma.202301856.

A partially dewetted liposome strategy has been developed to investigate the ability of phase separation of enzyme-functionalized elastin-like polypeptides into a crowded biomacromolecule's environment mimicking the cell cytoplasm. Thanks to osmotic pressure modulation, the characteristic cloud point temperature (T_{cp}) of ELPs could be tuned so that synthetic organelle compartments of an ELP-based multicomponent system with HRP as a model enzyme could be formed as a response to hyperosmotic stress. Such dynamic formation of membraneless organelles in a liquid-liquid phase separation mechanism represents an advance towards synthetic cell research as it brings together LLPS, compartmentalization and enzymes. The importance of the assembly of such synthetic organelles has been demonstrated to accelerate enzymatic reactions by locally increasing the enzyme concentration. This work proposes a unique approach to create protocellular systems with a new osmotic trigger to dynamically assemble intracellular synthetic organelle formation. It also represents a significant advance towards the construction and induction of complex cascade reactions in more realistic synthetic cells, promising to further our understanding of the importance and role of membraneless organelles in biological enzymatic reactions.

4. Experimental Section

Detailed presentation of the materials, equipment utilized, experimental procedures and characterization methods are provided in the Supporting Information. This contains the generation of partially dewetted liposomes from double emulsion microdroplets *via* microfluidics, construction of hypertonicity-induced organelle-like assemblies, assembly of enzymatically active synthetic organelles, and the study of biocatalytic synthetic organelles' capability of facilitating enzymatic reaction activity.

Statistical Analysis: For the determination of volume and corresponding concentration ratios of liposomes respectively, depending on the osmolarity of the hypertonic sucrose solutions, results were displayed as mean ± standard deviations. The sample sizes (n) were provided in the figure legends. The kinetics of enzymatic reactions from ELP-*b*-HRP and HRP respectively that were determined by the slope of the fluorescence intensity curves versus time were shown as mean ± standard deviations (n = 3 replicates). Concerning the measurements of T_{cp}, all data of derived count rate and the

Please cite this article as doi: 10.1002/adma.202301856.

fluorescence intensity increase for both ELP-*b*-HRP and HRP in shrinking vesicles were respectively normalized from 0 to 1 by using the software Origin (OriginLab Corp).

Supporting Information

Supporting Information is available from the Wiley Online Library or from the author.

Acknowledgements

C.S., H.Z. and S.L. gratefully acknowledge funding from IdEx Bordeaux (10-IDEX-03-02) and the European Union's Horizon 2020 research and innovation program under the Marie Skłodowska - Curie grant agreement (BIOMOLMACS, 859416). The authors thank Prof. Bertrand Garbay and Guillaume Goudounet for ELP[M_1V_3-40]-C gene construction and Pauline Coutand for its recombinant production in *Escherichia coli* bacteria.

Received: ((will be filled in by the editorial staff))
Revised: ((will be filled in by the editorial staff))
Published online: ((will be filled in by the editorial staff))

References

[1] J. W. Szostak, D. P. Bartel, P. L. Luisi, *Nature* **2001**, *409*, 387.

[2] a) R. Roodbeen, J. C. M. van Hest, *Bioessays* **2009**, *31*, 1299; b) P. A. Beales, B. Ciani, S. Mann, *Interface Focus* **2018**, *8*, 20180046; c) M. Marguet, C. Bonduelle, S. Lecommandoux, *Chem. Soc. Rev.* **2013**, *42*, 512.

[3] a) N.-N. Deng, M. Yelleswarapu, L. Zheng, W. T. S. Huck, *J. Am. Chem. Soc.* **2017**, *139*, 587; b) A. Peyret, E. Ibarboure, N. Pippa, S. Lecommandoux, *Langmuir* **2017**, *33*, 7079; c) R. J. R. W. Peters, M. Marguet, S. Marais, M. W. Fraaije, J. C. M. van Hest, S. Lecommandoux, *Angew. Chem. Int. Ed.* **2014**, *53*, 146.

Please cite this article as doi: 10.1002/adma.202301856.

[4] a) N. G. Moreau, N. Martin, P. Gobbo, T. Y. D. Tang, S. Mann, *Chem. Commun.* **2020**, *56*, 12717; b) W. Mu, Z. Ji, M. Zhou, J. Wu, Y. Lin, Y. Qiao, *Sci. Adv. 7*, eabf9000.

[5] C. P. Brangwynne, C. R. Eckmann, D. S. Courson, A. Rybarska, C. Hoege, J. Gharakhani, F. Jülicher, A. A. Hyman, *Science* **2009**, *324*, 1729.

[6] a) S. F. Banani, H. O. Lee, A. A. Hyman, M. K. Rosen, *Nat. Rev. Mol. Cell Biol.* **2017**, *18*, 285; b) D. Bracha, M. T. Walls, C. P. Brangwynne, *Nat. Biotechnol.* **2019**, *37*, 1435; c) J. Liu, F. Zhorabek, Y. Chau, *Matter* **2022**, *5*, 2787; d) A. A. Hyman, C. A. Weber, F. Jülicher, *Annu. Rev. Cell Dev. Biol.* **2014**, *30*, 39.

[7] W. Stroberg, S. Schnell, *Biophys. J.* **2018**, *115*, 3.

[8] M. B. Burg, J. D. Ferraris, N. I. Dmitrieva, *Physiol. Rev.* **2007**, *87*, 1441.

[9] a) C. Gao, J. Gu, H. Zhang, K. Jiang, L. Tang, R. Liu, L. Zhang, P. Zhang, C. Liu, B. Dai, J. Song, *Cell Rep.* **2022**, *40*, 111086; b) C. R. Boyd-Shiwarski, D. J. Shiwarski, S. E. Griffiths, R. T. Beacham, L. Norrell, D. E. Morrison, J. Wang, J. Mann, W. Tennant, E. N. Anderson, J. Franks, M. Calderon, K. A. Connolly, M. U. Cheema, C. J. Weaver, L. J. Nkashama, C. C. Weckerly, K. E. Querry, U. B. Pandey, C. J. Donnelly, D. Sun, A. R. Rodan, A. R. Subramanya, *Cell* **2022**, *185*, 4488; c) W. van Leeuwen, C. Rabouille, *Traffic* **2019**, *20*, 623; d) A. P. Jalihal, S. Pitchiaya, L. Xiao, P. Bawa, X. Jiang, K. Bedi, A. Parolia, M. Cieslik, M. Ljungman, A. M. Chinnaiyan, N. G. Walter, *Mol. Cell* **2020**, *79*, 978.

[10] a) C. Xu, N. Martin, M. Li, S. Mann, *Nature* **2022**, *609*, 1029; b) N.-N. Deng, W. T. S. Huck, *Angew. Chem. Int. Ed.* **2017**, *56*, 9736; c) H. Zhao, E. Ibarboure, V. Ibrahimova, Y. Xiao, E. Garanger, S. Lecommandoux, *Adv. Sci.* **2021**, *8*, 2102508; d) H. Zhao, V. Ibrahimova, E. Garanger, S. Lecommandoux, *Angew. Chem. Int. Ed.* **2020**, *59*, 11028; e) A. T. Rowland, D. N. Cacace, N. Pulati, M. L. Gulley, C. D. Keating, *Chem. Mater.* **2019**, *31*, 10243; f) J. W. Hindley, D. G. Zheleva, Y. Elani, K. Charalambous, L. M. C. Barter, P. J. Booth, C. L. Bevan, R. V. Law, O. Ces, *Proc. Natl. Acad. Sci.* **2019**, *116*, 16711; g) S. Deshpande, F. Brandenburg, A. Lau, M. G. F. Last, W. K. Spoelstra, L. Reese, S. Wunnava, M. Dogterom, C. Dekker, *Nat. Commun.* **2019**, *10*, 1800; h) H. Seo, H. Lee, *Nat. Commun.* **2022**, *13*, 5179; i) T. E. Miller, T. Beneyton, T. Schwander, C. Diehl, M. Girault, R. McLean, T. Chotel, P. Claus, N. S. Cortina, J.-C. Baret, T. J. Erb, *Science* **2020**, *368*, 649; j) S. Cao, L. C. da Silva, K. Landfester, *Angew. Chem. Int. Ed.* **2022**, *61*, e202205266.

[11] a) J. R. Simon, S. A. Eghtesadi, M. Dzuricky, L. You, A. Chilkoti, *Mol. Cell* **2019**, *75*, 66; b) A. Belluati, S. Thamboo, A. Najer, V. Maffeis, C. von Planta, I. Craciun, C. G. Palivan, W. Meier, *Adv. Funct. Mater.* **2020**, *30*, 2002949; c) R. Booth, Y. Qiao, M. Li, S. Mann, *Angew. Chem. Int. Ed.* **2019**, *58*, 9120; d) A. F. Mason, N. A. Yewdall, P. L. W. Welzen, J. Shao, M. van Stevendaal, J. C. M. van Hest, D. S. Williams, L. K. E. A. Abdelmohsen, *ACS Cent. Sci.* **2019**, *5*, 1360; e) C. L. Cuevas-Velazquez, T. Vellosillo, K. Guadalupe, H. B. Schmidt, F. Yu, D. Moses, J.

Please cite this article as doi: 10.1002/adma.202301856.

A. N. Brophy, D. Cosio-Acosta, A. Das, L. Wang, A. M. Jones, A. A. Covarrubias, S. Sukenik, J. R. Dinneny, *Nat. Commun.* **2021**, *12*, 5438.

[12] N.-N. Deng, M. A. Vibhute, L. Zheng, H. Zhao, M. Yelleswarapu, W. T. S. Huck, *J. Am. Chem. Soc.* **2018**, *140*, 7399.

[13] E. Rideau, R. Dimova, P. Schwille, F. R. Wurm, K. Landfester, *Chem. Soc. Rev.* **2018**, *47*, 8572.

[14] a) C. Vanhille-Campos, A. Šarić, *Soft Matter* **2021**, *17*, 3798; b) M. Yanagisawa, M. Imai, T. Taniguchi, *Phys. Rev. Lett.* **2008**, *100*, 148102.

[15] D. E. Meyer, A. Chilkoti, *Nat. Biotechnol.* **1999**, *17*, 1112.

[16] D. W. Urry, *J. Phys. Chem. B.* **1997**, *101*, 11007.

[17] a) R. Petitdemange, E. Garanger, L. Bataille, K. Bathany, B. Garbay, T. J. Deming, S. Lecommandoux, *Bioconj. Chem.* **2017**, *28*, 1403; b) Y. Xiao, Z. S. Chinoy, G. Pecastaings, K. Bathany, E. Garanger, S. Lecommandoux, *Biomacromolecules* **2020**, *21*, 114.

[18] a) S. B. Zimmerman, A. P. Minton, *Annu. Rev. Biophys. Biomol. Struct.* **1993**, *22*, 27; b) C. D. Keating, *Acc. Chem. Res.* **2012**, *45*, 2114.

[19] P. Baumann, M. Spulber, O. Fischer, A. Car, W. Meier, *Small* **2017**, *13*, 1603943.

[20] A. Belluati, I. Craciun, J. Liu, C. G. Palivan, *Biomacromolecules* **2018**, *19*, 4023.

[21] H. Bisswanger, *Perspect. Sci.* **2014**, *1*, 41.

[22] W. M. Aumiller, Jr., B. W. Davis, E. Hatzakis, C. D. Keating, *J. Phys. Chem. B.* **2014**, *118*, 10624.

[23] R. Chong, J.-E. R. Rho, H.-J. Yoon, P. S. Park, T.-H. D. Rho, J. Y. Park, L. Park, Y.-H. Kim, J. H. Lee, *Talanta* **2013**, *116*, 403.

Please cite this article as doi: 10.1002/adma.202301856.

To mimic the dynamic assembly of intracellular stress membraneless organelles inside living cells, elastin-like polypeptide-derived components are encapsulated within partially dewetted liposomes and can respond rapidly to hyperosmotic stress by undergoing fast phase separation to assemble biofunctional synthetic organelles. These synthetic organelles are enzymatically active and are capable of controlling the rate of enzymatic reactions by locally segregating the enzyme and substrate.

Clémence Schvartzman, Hang Zhao*, Emmanuel Ibarboure, Vusala Ibrahimova, Elisabeth Garanger, Sébastien Lecommandoux*

Control of Enzyme Reactivity in Response to Osmotic Pressure Modulation Mimicking Dynamic Assembly of Intracellular Organelles

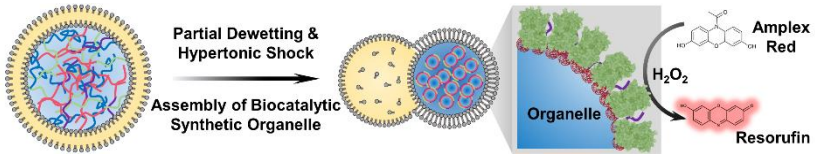

Please cite this article as doi: 10.1002/adma.202301856.

Supporting Information

Control of Enzyme Reactivity in Response to Osmotic Pressure Modulation Mimicking Dynamic Assembly of Intracellular Organelles

Clémence Schvartzman, Hang Zhao, Emmanuel Ibarboure, Vusala Ibrahimova, Elisabeth Garanger, Sébastien Lecommandoux**

Table of Contents

Part I. Supplementary Experimental Section and Characterization Methods

Materials: Poly(ethylene glycol) (PEG, 6 kDa) polymer was purchased from Alfa Aesar. Poly(vinyl alcohol) (PVA, 13-23 kDa, 87-89% hydrolyzed) polymer, sucrose (GC, 95.5%), sigmacote, 3-aminopropyltriethoxysilane (APTES, 98%), ampliflu™ red (HPLC grade, 96%), 2,2'-azino-bis(3-ethylbenzothiazoline-6-sulfonic acid (ABTS, HPLC grade, 98%), resorufin (95%), the enzyme of horseradish peroxidase (HRP, hydrophilized powder, 150 U mg^{-1}), the heterobifunctional cross-linker 4-(*N*-maleimidomethyl)cyclohexane-1-carboxylic acid 3-sulfo-*N*-hydroxysuccinimide ester sodium salt (sulfo-SMCC) and *N*,*N*-diisopropylethylamine (DIPEA) were purchased from Sigma-Aldrich. L-α-phosphatidylcholine (Egg PC, 25 mg ml^{-1} in chloroform) was bought from Avanti Polar Lipids. Pluronic® F-68 was obtained from Gibco. Hydrogen peroxide (H_2O_2, 35%) was purchased from Acros. All compounds were used without further purification. The following solvent were purchased from Sigma-Aldrich and used without further purification: chloroform (anhydrous, 99%), hexane (anhydrous, 95%) and dimethyl sulfoxide (DMSO, 99.9%). Water with a resistivity of 18.2 MΩ cm^{-1} was prepared using a Millipore Milli-Q system.

Microfluidics: To generate water-in-oil-in-water double emulsions, a capillary-based microfluidic device was utilized.[1] To make the co-flow microfluidic device, two cylindrical capillaries of inner diameter 580 μm and outer dimension 1 mm (World precision instruments, 1B100-4) were tapered by a micropipette puller (Sutter instrument, P-97) followed by polishing the orifices with sand papers into 60 μm and 120 μm, respectively. The capillary with smaller orifice treated by sigmacote into hydrophobic was used for injection innermost aqueous phase, while surface of the larger-sized capillary was rendered into hydrophilic by APTES and used as the collection channel. A square capillary (VitroCom, 2956C1) was used to nest both cylindrical capillaries that were inserted in opposite direction. Lastly, dispensing needles used as inlets of fluids were connected at the junctions between capillaries by using a transparent 5 min Epoxy (Devcon). The devices were connected to high-precision syringe pumps (Chemyx, Fusion 100) *via* polyethylene tubing (Scientific Commodities Inc., BB31695-PE/4) to ensure reproducible, stable flows.

Formation of double-emulsion microdroplets and their transformation to partially dewetted liposomes: Typically, to create water-in-oil-in-water double-emulsion microdroplets for studying hyperosmotic stress-induced formation of synthetic organelles, an aqueous phase - 8

wt% PEG phase containing 0.25 mg ml^{-1} of rhodamine-labelled ELP-*b*-PEG was flowed in the injection capillary as innermost solution. An organic mixture of chloroform and hexane (36:64 vol%) containing 5 mg mL^{-1} of Egg PC was used as middle phase and was injected through the interstices between the injection and square capillaries, whereas the continuous phase of 10 wt% PVA with 0.2% F-68 was pumped through the interstices between the collection and square capillaries. Typical flow rates were set to 500, 1000 and 8000 μL h^{-1} for inner, middle and outer phases, respectively. These three phases produced double-emulsion microdroplets at the junction, which then flowed along the collection capillary and were collected and sealed with a cover slip in a cavity glass slide (BRAND®). Observations of transformation of W/O/W double emulsions to partially dewetted liposomes were made after 15 mins since fresh microdroplets were collected. The oil phase that initially surrounds the inner aqueous lumen gradually underwent dewetting process with the assistance of F-68, forming a lipid reservoir which remained attach to the lipid vesicles.

Bioproduction, isolation and purification of ELP[M_1V_3-40], ELP[M_1V_3-40]-Cysteine, ELP[M_1V_3-60] and ELP-b-PEG bioconjugate: ELP[M_1V_3-40], ELP[M_1V_3-40]-Cysteine and ELP[M_1V_3-60] were produced by recombinant DNA and protein engineering techniques in *E. coli* and isolated using previously reported procedures.[2] The bioconjugate of ELP-*b*-PEG was produced and isolated as previously presented by our group elsewhere.[3]

Synthesis of ELP-b-HRP conjugate: **Step 1** - 0.2 μl of DIPEA (1.2 μmol, 2 equiv.) was added to a solution of HRP (23 mg, 0.6 μmol, 1 equiv.) in phosphate buffer saline (PBS) pH 7.4 (10 mg ml^{-1}) and stirred for 15 min. 3 mg of cross-linker sulfo-SMCC (6 μmol, 10 equiv.) was dissolved in 100 μl of DMF and added dropwise to the reaction mixture. The reaction mixture was stirred at ambient temperature for 4 hours. The excess sulfo-SMCC was afterwards removed by washing (5 times) the solution with PBS pH 7.4 in centrifuge filters (Amicon Ultra-15, 10kDa); **Step 2** - ELP[M_1V_3-40]-Cysteine (20 mg, 1.2 μmol, 2 equiv.), presenting a *C*-terminal cysteine residue (Figures S4b, Figure S5), was dissolved in PBS pH 7.4 at 10 mg ml^{-1} at 4 °C. The solution of HRP-Mal from Step 1 was added. The mixture was incubated in a thermomixer at 10 °C for 24 hrs. The reaction mixture was transferred into 0.5 ml centrifuge filters (Amicon Ultra, 10kDa) and washed (5 times) with ultrapure water. The final solution was lyophilized to yield 35 mg of ELP-*b*-HRP conjugate. The conjugate was analyzed by MALDI-MS to estimate the average number of ELP chains conjugated to the HRP. Since HRP contains 4 primary amine groups (*N*-terminal end and ^{174}Lys, ^{232}Lys and ^{241}Lys residues),[4]

(Figure S4a) the ELP-*b*-HRP conjugate may contains up to 4 ELPs. The molar masses of all possible conjugates are provided in the table below:

Compound	Molar mass (kDa)
ELP	17
HRP	40
ELP-*b*-HRP	57
ELP_2-*b*-HRP	74
ELP_3-*b*-HRP	91
ELP_4-*b*-HRP	109

From the relative intensity of the different species detected on the mass spectrum of the ELP-*b*-HRP conjugate, it was estimated that HRP was conjugated to 2 ELPs on average (Figure S6).

Mass-spectrometry analyses: MALDI-MS spectra were performed by the CESAMO (Bordeaux, France) on an AutoflexmaX TOF mass spectrometer (Bruker Daltonics, Bremen, Germany) equipped with a frequency tripled Nd:YAG laser emitting at 355 nm. Spectra were recorded in the positive-ion mode and with an accelerating voltage of 19 kV. Samples were dissolved either in a mixture of water and acetonitrile (1:1) or in pure water at 10 mg ml^{-1}. Sinapinic acid matrix was prepared as a supersaturated solution (ca.10 mg ml^{-1}) in a mixture of water/acetonitrile/trifluoroacetic acid (49.9:50:0.1). The solutions were combined in a 20:2 or 18:2 volume ratio of matrix to sample. 1.5 to 2 µl of the resulting solution were deposited onto the sample target and vacuum-dried.

Confocal microscopy imaging: Microdroplets were collected on a glass slide with a single cavity and subsequently sealed with a coverslip for the dewetting process to take place. Then, 7 µl of vesicles and the solution of 1 $_M$ sucrose and 0.2% F-68 solution were injected into an imaging chamber (Ibidi GmbH, Germany) to induce the assembly of the synthetic organelles. To validate the dynamic reversibility of organelle-like constructs, a water phase of 0.2% F-68 was carefully added to the imaging chamber. Regarding the enzymatic reaction, a following 225 μ_M H_2O_2 solution was injected in the imaging chamber to start the reaction. Images and videos were acquired by a confocal laser scanning microscopy (Leica, SP5 AOBS) through an HCX PL APO 10× dry objective. To assess localization of ELP-*b*-PEG and ELP[M_1V_3-60] and monitor their coacervation and spatial distribution, they were labeled with spectrally different fluorophores. A diode laser (561 nm) and He-Ne (633 nm) ion laser were used to excite rhodamine and BODIPY, respectively. To avoid an artifact of visualizing rhodamine-labeled

ELP-*b*-PEG and BODIPY-labeled ELP[M_1V_3-60], sequential imaging mode was used to reduce fluorescence crosstalk among various fluorophores. In addition, the diode laser (561 nm) was also used to excite the product – resorufin from the enzymatic reaction. All imaging acquisitions were made at room temperature (23 ℃).

Measurement of the diameter of lipid vesicles and determination of concentrations after hyperosmotic stress: The diameter of shrunken and normal lipid vesicles was analyzed by a software ImageJ.[5] The initial diameter and encapsulant concentration are denoted as D_i and C_i, respectively; the eventual diameter and encapsulant concentration are D_{ii} and C_{ii}. Because salt (or polymer) cannot transfer across the bilayer membrane, the total amount of salt (or polymer) molecules keeps the same inside the inner water compartment. Therefore, we can get

$$\frac{4}{3}\pi\left(\frac{D_i}{2}\right)^3 \times C_i = \frac{4}{3}\pi\left(\frac{D_{ii}}{2}\right)^3 \times C_{ii} \qquad \text{(Equation S1)}$$

$$C_{ii} = C_i \times \left(\frac{D_i}{D_{ii}}\right)^3 \qquad \text{(Equation S2)}$$

Consequently, the final dimension of liposomes can be easily predicted and tuned via changing the applied hyperosmotic pressure. The volumes were then determined, and shrinkage factor was calculated. The initial concentrations were then multiplied by the shrinkage factor to determine concentrations in shrunken liposomes.

Determination of transition temperature (T_{cp}) of ELP-based derivatives by dynamic light scattering (DLS): To determine the transition temperature (T_{cp}) of several ELP-based conjugates in solution, dynamic light scattering (DLS) measurements were performed on NanoZS instrument (Malvern, U.K.) at a 173° angle, at a constant position in the cuvette (constant scattering volume). The derived count rate (DCR) was defined as the mean scattered intensity normalized by the attenuation factor. The DCR was plotted against temperature and the T_{cp} is defined as the temperature corresponding to the point where the DCR starts increasing on the plot. Measurements were carried out simulating both the inside environment of a vesicle and the conditions before/after a hypertonic shock. Temperature ramps were typically performed from 5 °C to 50 °C for all conditions.

Crowding effect of the macromolecule PEG on the Michaelis-Menten parameters: To show the crowding effect of PEG, the kinetics analysis upon systems containing either ELP-*b*-HRP or

free HRP were assessed in water and PEG respectively by varying the cofactor concentration, H_2O_2. Experiments were carried out in bulk, at 23 °C. Solutions were prepared and reached final concentrations of 0.054 n_M HRP, 75 μ_M amplex red and 8 wt% PEG. The enzymatic reactions were initiated using H_2O_2 with final concentrations reaching [15 μ_M], [10 μ_M], [7.5 μ_M], [5 μ_M] and [2.5 μ_M] respectively. The fluorescence intensity *vs* time plot was obtained. Then, a calibration curve of the average fluorescence intensity *vs* the resorufin concentration was constructed. The fluorescence intensity could therefore be replaced by its equivalence in resorufin concentration over time. From this graph, the initial rates of reaction were determined by measuring the slope of the curve. By plotting the initial reaction rates *vs* the cofactor concentration, the Michaelis-Menten curves were obtained. Finally, the Lineweaver-Burk plots were constructed by taking 1/reaction rate *vs* 1/[H_2O_2]. From these graphs, the Michaelis-Menten constant K_m was determined using the following equation:

$$\frac{1}{V_0} = \frac{K_m}{V_{max}} \times \frac{1}{[S]} + \frac{1}{V_{max}} \qquad \text{(Equation S3)}$$

Where V_0 is the initial velocity of the enzyme, K_m is the Michaelis-Menten constant, V_{max} is the maximum velocity at saturating concentration, [S] is the concentration of the substrate. The Specific Activity (*S.A.*) of the enzyme was determined using the following equation:

$$S.A. = \frac{\text{moles of substrate transformed}}{\text{min} \times \text{total weight of enzyme}} \qquad \text{(Equation S4)}$$

All value were presented in Table 1 in the manuscript.

Determination of kinetics of enzymatic reactions in bulk by fluorescence spectrofluorometer: Measurements were carried out in bulk, in a high precision quartz glass cell from Hellma Analytics, simulating both the inside environment of a vesicle and the conditions before/after a hyperosmotic stress. As the initial and final volumes of the vesicles were known, it was possible to determine the final concentration of each of the components in the vesicles after shrinking. Experiments were conducted at 23 °C. All the compounds constituting the solutions were thoroughly mixed in an Eppendorf tube and pipetted into the cuvette. Lastly, 1 m_M H_2O_2 stock solution was added and quickly mixed through the solution, before starting running the measurement of monitoring increase of fluorescence intensity. Each experiment was repeated three times. To conduct these experiments, the fluorescence spectrometer (Jasco FP-8500) was used in the course measurement mode. To detect the produced resorufin, excitation and emission wavelength were set at 470 and 590 nm respectively.

Determination of kinetics of enzymatic reactions in bulk via using UV-Vis spectrophotometer: To reinforce the results observed using the spectrofluorometer, the same experiments were conducted in an Agilent Cary 100 UV-Vis spectrophotometer, using ABTS as an alternative reagent. In the presence of H_2O_2 and the enzyme HRP, ABTS can be oxidized to a radical cation with absorption at 405 nm. This method is however less sensitive than the spectrofluorometer, and ABTS is readily oxidized and has a slow fluorescence response compared to amplex red.

Kinetics of enzymatic reactions in partially dewetted liposomes followed by confocal microscopy: Once the protocol and parameters were established in the quartz cuvette, the experiments were conducted inside the lipid vesicles, which were achieved via the microfluidics system. The production of resorufin was followed by confocal microscopy. A ten-fold higher concentration of both ELP-*b*-HRP and HRP (compared to bulk phase analysis) was encapsulated in the vesicles due to sensitivity differences between the spectrofluorometer and the confocal microscope. A time-series imaging mode was set for monitoring the production of resorufin over time.

Part II. Supplementary Figures S1-S11 and Table S1

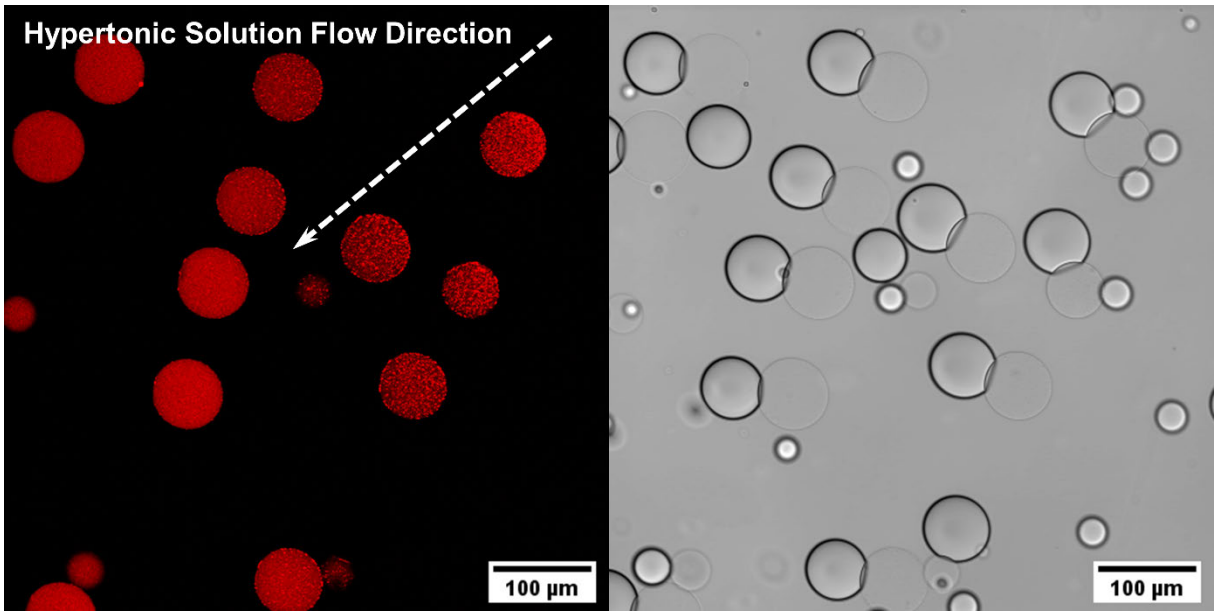

Figure S1. Gradual assembly of synthetic organelles from ELP-*b*-PEG bioconjugates as soon as the hypertonic solution diffuses across partially dewetted liposomes.

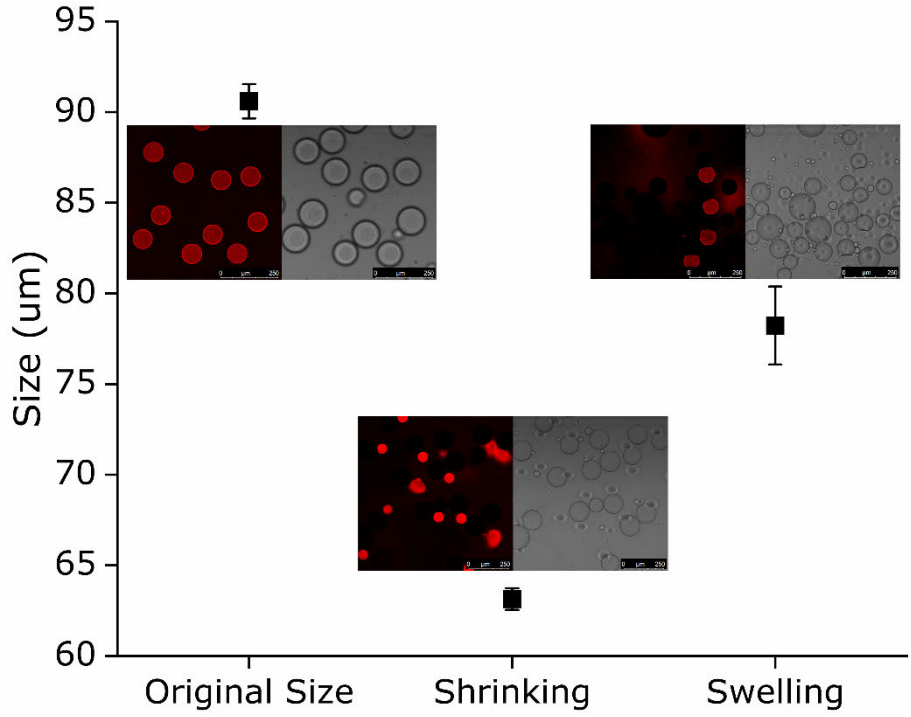

Figure S2. Confocal images and size measurements of partially dewetted lipid vesicles in the shrinking and swelling process in the hyperosmotic and hypoosmotic stress solutions respectively.

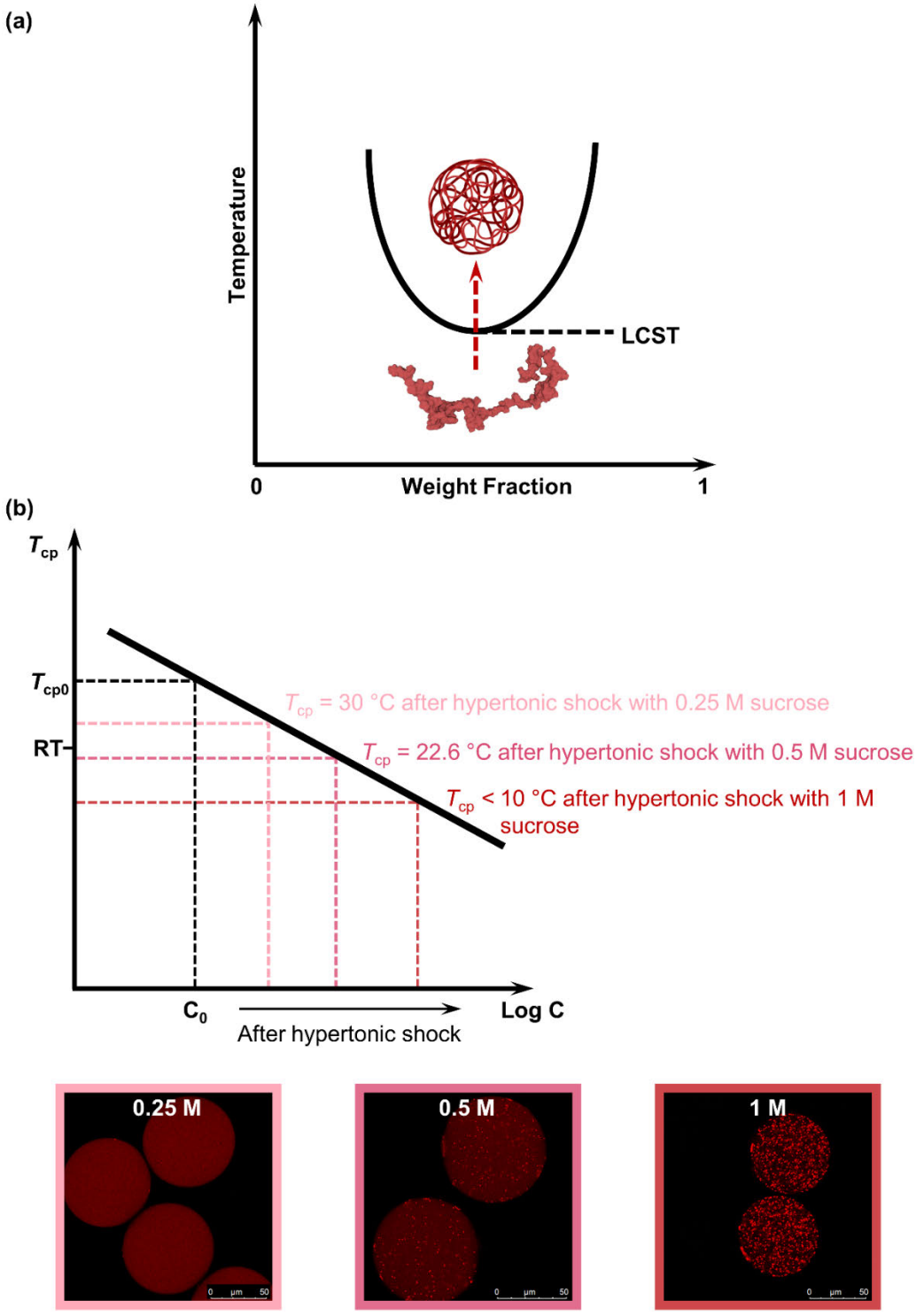

Figure S3. (a) ELPs exhibit a LCST behavior: at a specific concentration, below their cloud point temperature (T_{cp}), ELPs are water soluble and present as random coil chains; above T_{cp}, ELPs dehydrate and form coacervates. (b) Schematic illustration of the evolution of the T_{cp} of the ELP-*b*-PEG bioconjugate as a function of concentration. Hyperosmotic stress applied onto liposome-based artificial cells induce an isothermal concentration increase and therefore the assembly of rhodamine-labeled ELP-*b*-PEG chains into membraneless organelle mimics.

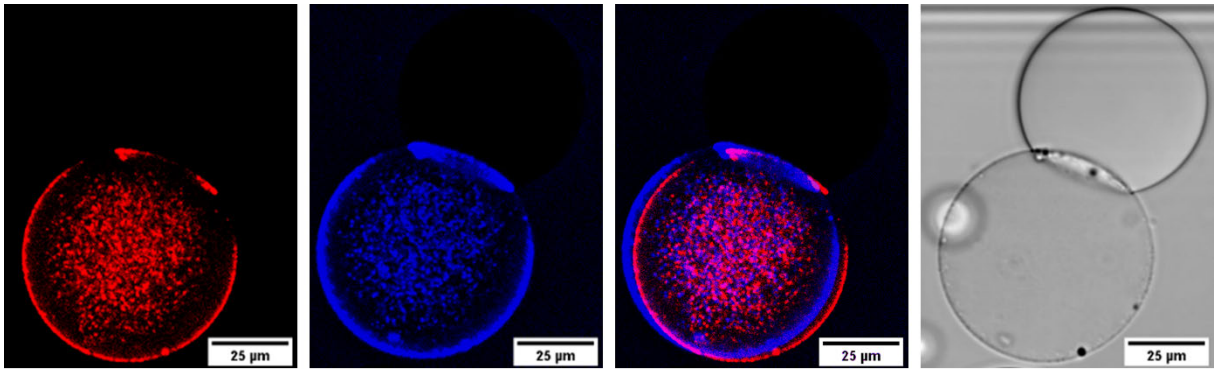

Figure S4. Representative confocal microscopy images of synthetic organelle-like assemblies from ELP-based multicomponent system (BDP-ELP + ELP-*b*-PEG) within a shrunken partially dewetted lipid vesicle; red color indicates ELP-*b*-PEG and blue indicates BDP-ELP.

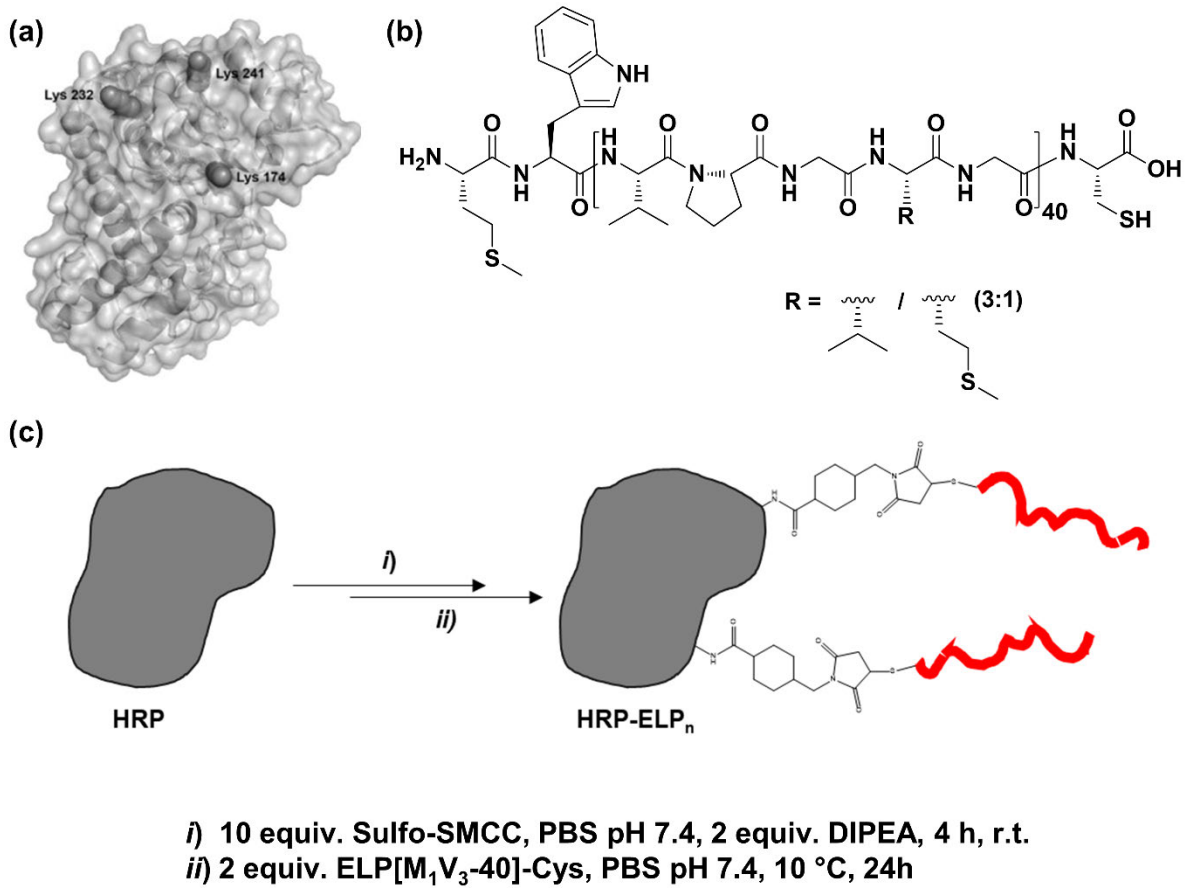

***i*) 10 equiv. Sulfo-SMCC, PBS pH 7.4, 2 equiv. DIPEA, 4 h, r.t.**
***ii*) 2 equiv. ELP[M_1V_3-40]-Cys, PBS pH 7.4, 10 °C, 24h**

Figure S5. (a) 3D representation of the average structure of HRP, showing 3 exposed Lys residues.[4] (b) Chemical structure of ELP[M_1V_3-40]-C. (c) Synthetic scheme and conditions to access the ELP-*b*-HRP conjugate.

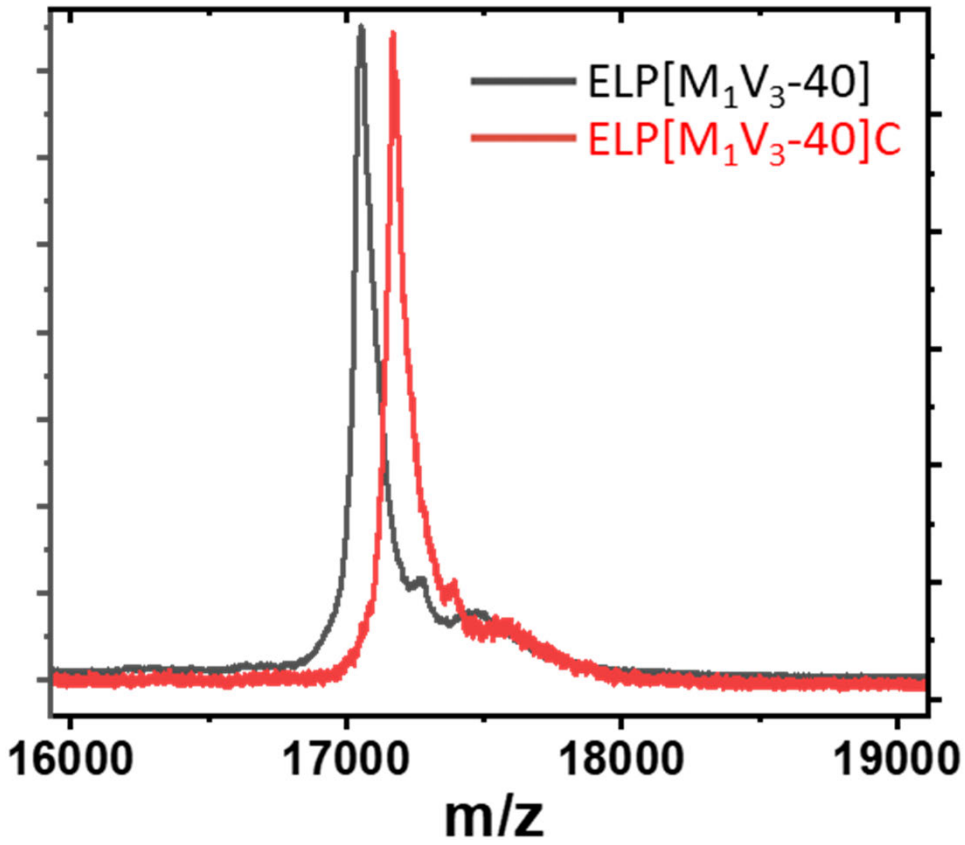

Figure S6. Superimposed MALDI mass spectra of ELP[M_1V_3-40] and ELP[M_1V_3-40]-C.

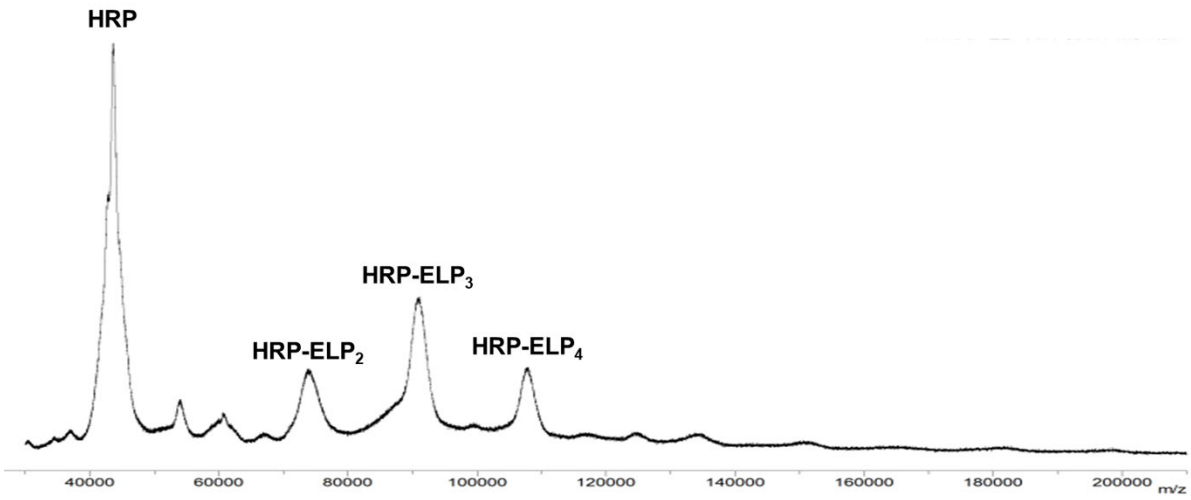

Figure S7. MALDI mass spectrum of ELP-*b*-HRP conjugate.

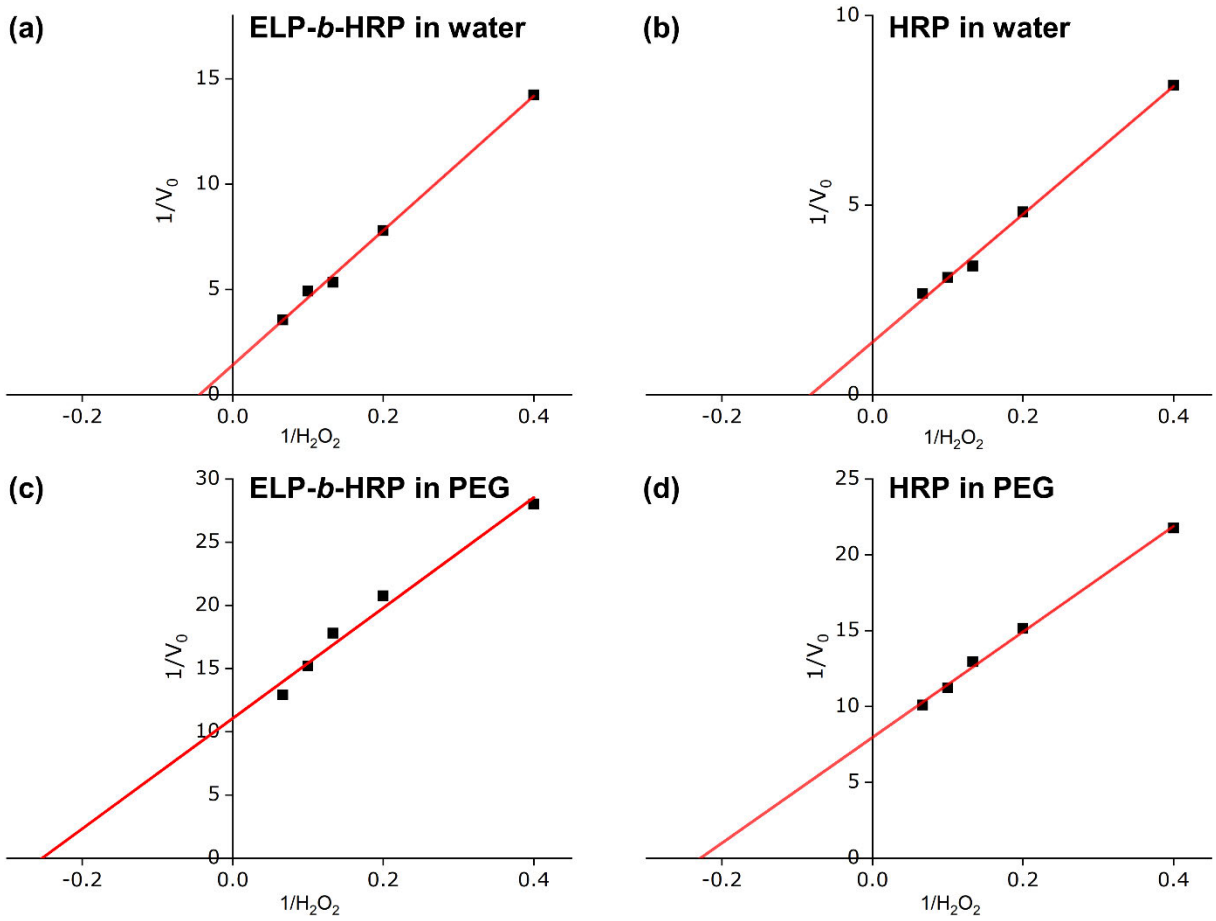

Figure S8. Lineweaver-Burk plots. Lineweaver Burk plots of ELP-*b*-HRP and HRP in water and PEG solution, respectively. The Michaelis Menten constant (K_m) of each condition was determined at the interception of the x axis, where x is $-1/K_m$.

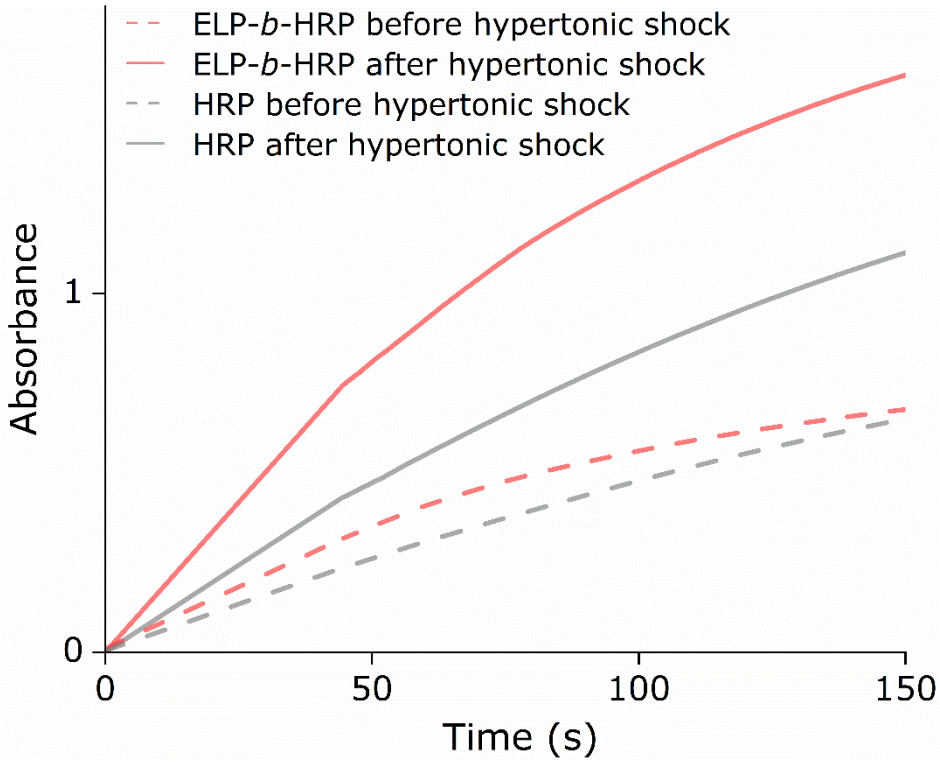

Figure S9. Kinetics of the enzymatic reaction using an alternative chemical substrate of ABTS determined by UV-Vis spectrometry.

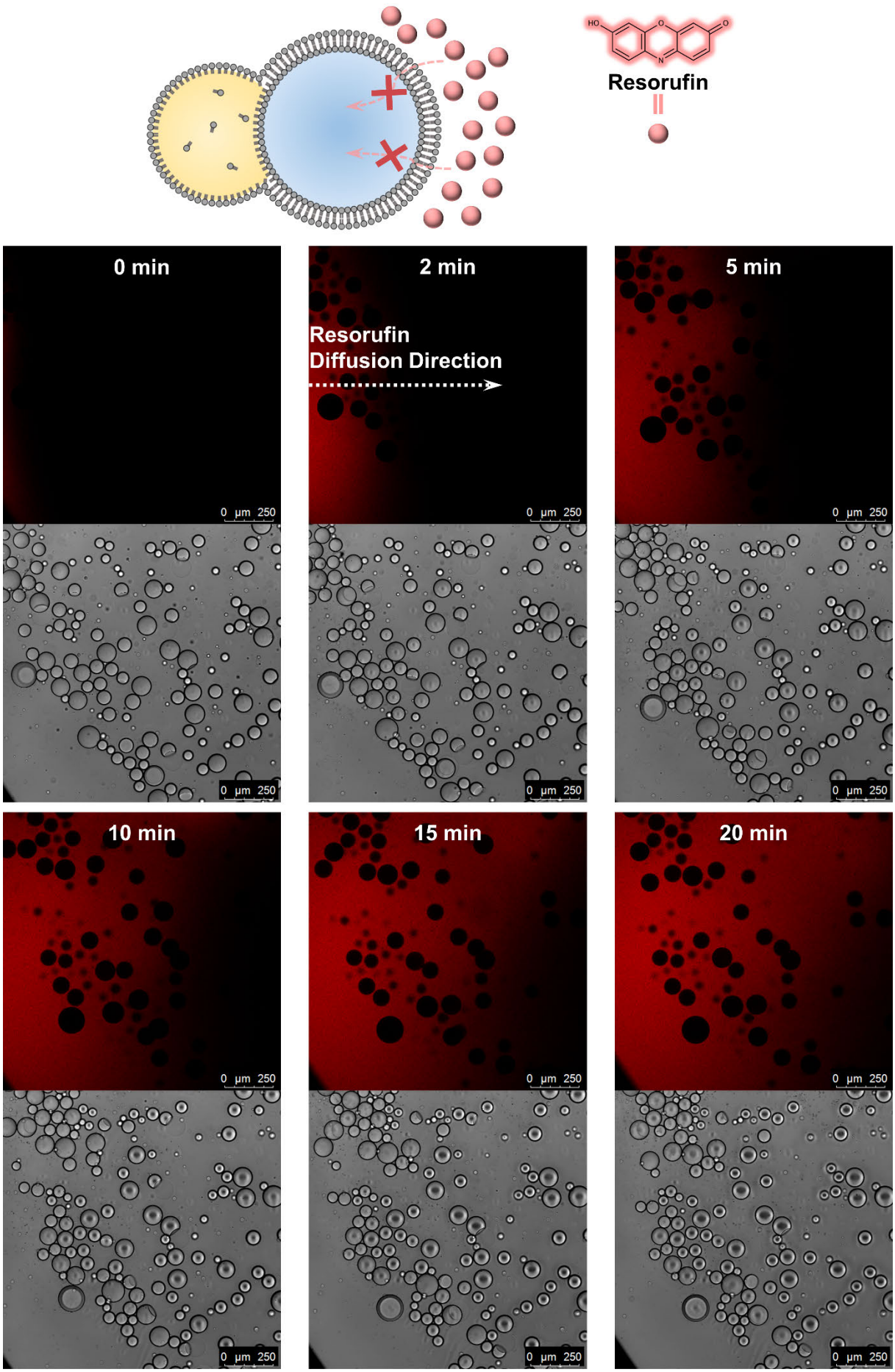
Resorufin
0 min
2 min
Resorufin
Diffusion Direction
5 min
10 min
15 min
20 min
0 µm 250

Figure S10. Permeability tests of the membrane towards resorufin. Illustration of non-permeable membranes to resorufin diffusing in the outer medium. Time series of confocal images (bright field and red channel) of monitoring resorufin diffusing in the sample. To assess the non-permeability of the membranes towards resorufin, partially dewetted liposomes, which have not been subjected to a hypertonic shock, were injected into an observation chamber and submitted to resorufin diffusion in the sample. After 20 min of observation, no resorufin was found to diffuse inside vesicles.

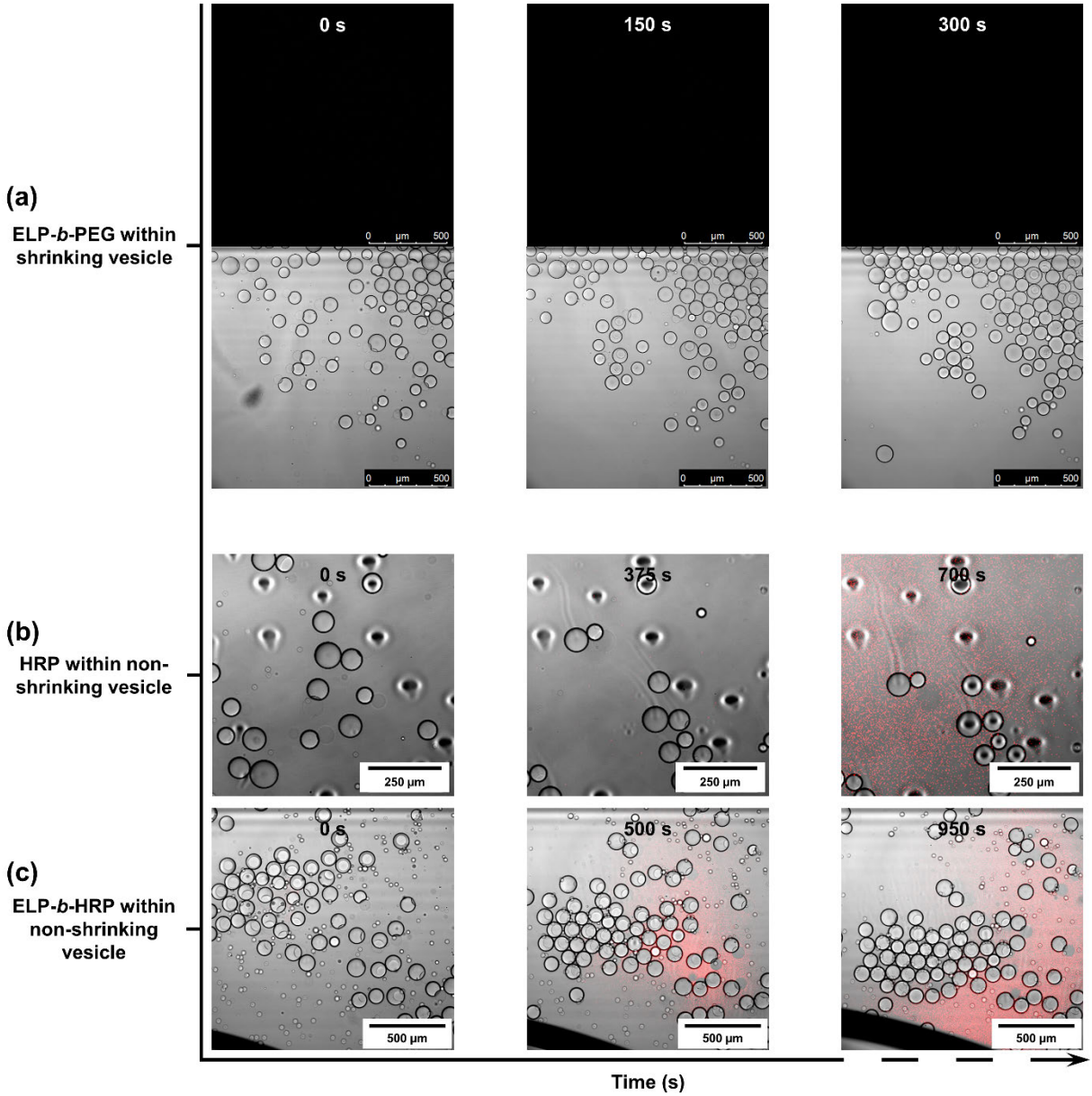

Figure S11. Enzymatic reaction of producing resorufin from amplex red in the absence/presence of the enzyme within shrinking or non-shrinking partially dewetted liposomes. (a) As a control, ELP-*b*-PEG to replace either free HRP or ELP-*b*-HRP was encapsulated inside the vesicles in the microfluidics process. 7 µL of partially dewetted vesicles were injected in an

observation chamber, followed by an addition of 1 m_M H_2O_2 solution. The overall sample was monitored for 300 s, without any detection of resorufin, proving that the HRP enzyme is needed to catalyze the reaction of producing resorufin. (b) HRP and (c) ELP-*b*-HRP were encapsulated respectively into liposomes which were not subjected to a hyperosmotic shock. Both of enzymatic reactions were monitored for over 10 min, without any visually imperceptible increase in fluorescence intensity being detected inside liposomes. The red background appeared over time as some vesicles bursted, releasing their inner content of amplex red and HRP/ELP-*b*-HRP, reacting with H_2O_2 and subsequently forming resorufin.

Table S1. Solution composition for spectrofluorescence analysis.

	Single HRP Before hypertonic shock	Single HRP After hypertonic shock	ELP-*b*-HRP Before hypertonic shock	ELP-*b*-HRP After hypertonic shock
HRP	0.054 n_M*	0.14 n_M	-	-
ELP-*b*-HRP	-	-	0.054 n_M*	0.14 n_M
ELP-*b*-PEG	-	-	0.125 mg ml^{-1}	0.325 mg ml^{-1}
BDP-ELP	-	-	0.250 mg ml^{-1}	0.65 mg ml^{-1}
Amplex Red	75 μ_M	195 μ_M	75 μ_M	195 μ_M
PEG	8 wt%	20.8 wt%	8 wt%	20.8 wt%
H_2O_2	75 μ_M	75 μ_M	75 μ_M	75 μ_M

*In the spectrofluorometer analysis, the concentration is 0.054 n_M for both free HRP and ELP-*b*-HRP, while in the scenario of inducing enzymatic reaction within partially dewetted liposomes, the concentration for both free HRP and ELP-*b*-HRP is increased by 10-fold to 0.54 n_M.

Part III. Supplementary Videos S1

Video S1. Enzymatic reaction within shrunken partially dewetted liposomes catalyzed either by HRP alone or by ELP-*b*-HRP.

Part IV. Supplementary References

[1] A. S. Utada, E. Lorenceau, D. R. Link, P. D. Kaplan, H. A. Stone, D. A. Weitz, *Science* **2005**, *308*, 537.

[2] a) R. Petitdemange, E. Garanger, L. Bataille, K. Bathany, B. Garbay, T. J. Deming, S. Lecommandoux, *Bioconj. Chem.* **2017**, *28*, 1403; b) R. Petitdemange, E. Garanger, L. Bataille, W. Dieryck, K. Bathany, B. Garbay, T. J. Deming, S. Lecommandoux, *Biomacromolecules* **2017**, *18*, 544.

[3] Y. Xiao, Z. S. Chinoy, G. Pecastaings, K. Bathany, E. Garanger, S. Lecommandoux, *Biomacromolecules* **2020**, *21*, 114.

[4] N. Mogharrab, H. Ghourchian, M. Amininasab, *Biophys. J.* **2007**, *92*, 1192.

[5] J. Schindelin, I. Arganda-Carreras, E. Frise, V. Kaynig, M. Longair, T. Pietzsch, S. Preibisch, C. Rueden, S. Saalfeld, B. Schmid, J.-Y. Tinevez, D. J. White, V. Hartenstein, K. Eliceiri, P. Tomancak, A. Cardona, *Nat. Methods* **2012**, *9*, 676.